Actin protects mammalian eggs against chromosome segregation errors

Binyam Mogessie and Melina Schuh*

Department of Meiosis, Max Planck Institute for Biophysical Chemistry, Am Fassberg 11, 37077 Göttingen, Germany

*Correspondence: melina.schuh@mpibpc.mpg.de (M.S.)

One Sentence Summary: Actin prevents chromosome segregation errors by promoting the formation of functional kinetochore fibers.

Abstract

Chromosome segregation is driven by a spindle that is made of microtubules, but is generally thought to be independent of actin. Here, we report an unexpected actin-dependent mechanism that drives the accurate alignment and segregation of chromosomes in mammalian eggs. Prominent actin filaments permeated the microtubule spindle in eggs of several mammalian species, including humans. Disrupting actin in mouse eggs led to significantly increased numbers of misaligned chromosomes as well as lagging chromosomes during meiosis I and II. We found that actin drives accurate chromosome segregation by promoting the formation of functional kinetochore-fibers, the microtubule bundles that align and segregate the chromosomes. Thus, actin is essential to prevent chromosome segregation errors in eggs, which are a leading cause of miscarriages, infertility and Down Syndrome.

Chromosome segregation is well-established to be driven by a spindle that consists of microtubules. The microtubules first capture and align the chromosomes at the spindle center. During anaphase, the chromosomes are segregated and move to the spindle poles. The movement of chromosomes is driven by the shortening of microtubule bundles that are attached to the chromosomes' kinetochores (*1, 2*). These kinetochore fibers (k-fibers) cooperate with a large number of microtubule-associated motor and non-motor proteins to align and segregate the chromosomes (*3, 4*). Although actin has been reported in spindles of various species, it is generally not thought to be involved in chromosome segregation (*5*).

The reliable segregation of chromosomes is of particular importance during meiosis, the specialized cell division that leads to the formation of eggs and sperm. The egg and the sperm need to have precisely one copy of each chromosome to give rise to a healthy embryo upon fertilization. But surprisingly, human eggs frequently contain an incorrect number of chromosomes. Depending on the age of the woman, around 10-50% of eggs are chromosomally abnormal (*6-8*). This makes aneuploidy in human eggs the most common cause of pregnancy losses and several genetic disorders such as Down Syndrome (*9-11*).

Aneuploidy in eggs arises from chromosome segregation errors during the meiotic divisions of the egg's progenitor cell, the oocyte (*11, 12*). Oocytes are stored in the ovary for prolonged periods, where they are arrested in prophase of the first meiotic division (*13*). Once every menstrual cycle, an oocyte resumes meiosis and matures into a fertilizable egg. First, the nuclear envelope breaks down and a microtubule spindle assembles in the center of the oocyte. Next, the spindle aligns the chromosomes at its equator and moves to the oocyte surface. It then segregates the homologous chromosomes during anaphase I and eliminates half of them into a very small cell, the polar body. Subsequently, the metaphase II spindle assembles and aligns the other half of the chromosomes at its equator. The egg then stays arrested in metaphase II until it is fertilized. Upon fertilization, the sister chromatids are segregated during anaphase II and half of them are eliminated into a second polar body. This completes the second meiotic division. In the newly formed and genetically unique embryo, two pronuclei assemble that contain the male and female DNA, and the mitotic divisions of the embryo begin (*13*). The mechanisms that drive and control chromosome segregation during the two meiotic divisions as well as the causes of high levels of aneuploidy in meiosis are still incompletely understood.

Results

Actin filaments permeate the microtubule spindle in oocytes of many mammals, including humans

We found prominent actin filaments in spindles of human, mouse (*14, 15*), porcine and ovine eggs by staining actin with fluorescent phalloidin (Fig. S1A). The filaments permeated the entire spindle volume and formed structures that resembled a microtubule spindle. We will refer to these actin structures as spindle actin throughout the manuscript. The wide conservation of spindle actin suggested that it has an essential function, which we set out to investigate.

Spindle actin assembled gradually during the first meiotic division in mouse oocytes and became most prominent when the homologous chromosomes segregated during anaphase I: dense, long actin bundles that spanned the entire spindle length permeated

the microtubule spindle throughout anaphase (Fig. 1A, movies S1 and S2). Super-resolution imaging of actin, microtubules and chromosomes upon drug-induced microtubule depolymerization revealed that spindle actin is microtubule-dependent (Fig S2, A and B, and movie S3). The prominence of spindle actin during anaphase suggested a potential role in chromosome segregation. To investigate this possibility, we examined the behavior of chromosomes and microtubules in the presence and absence of spindle actin in live oocytes.

Actin prevents lagging chromosomes during anaphase I

Spindle actin was disrupted by two different approaches: isolation of oocytes from *Fmn2*$^{-/-}$ mice, in which lack of the actin nucleator Formin-2 disrupts spindle actin (*14, 15*) (Fig. 1C), as well as treatment of oocytes with the actin-depolymerizing drug Cytochalasin D (Fig. 1B and S3, movies S4 and S5). Disruption of actin had no notable effect on the timing of meiotic maturation events (Fig. S4A), alignment of homologous chromosomes on the metaphase I spindle (Fig. S4B), efficiency of anaphase I onset (Fig. S4C) or spindle elongation during anaphase I (Fig. S4, D and E). Thus, oocytes are generally healthy and capable of progressing through meiosis when actin is absent. But strikingly, oocytes were significantly more likely to show chromosome segregation defects during anaphase I: instead of segregating all chromosomes simultaneously, individual chromosomes were frequently lagging behind the two main masses of chromosomes (movies S6-S9). The overall speed of chromosome movement was also reduced (Fig. 2, C and F).

Oocytes were scored to have mildly or severely lagging chromosomes, when individual chromosomes were still separated from the main chromosome mass 12 or 18 minutes after anaphase onset, respectively (Fig. 2A). These manual quantifications (Fig. 2, B and D, E and G, S5A) as well as the automated detection of lagging chromosomes in Imaris (Fig. S5, G and H) confirmed that disruption of actin led to a significant increase in chromosomes which moved more slowly than the two main chromosome masses.

Formin-2 also nucleates a network of actin filaments in the cytoplasm that transports Rab11a-positive vesicles and mediates asymmetric spindle positioning in mouse oocytes (*14-17*). Thus, we tested if the lack of actin-dependent transport in *Fmn2*$^{-/-}$ oocytes

contributes to chromosome segregation errors. The formation of Rab11a-positive vesicles and their transport along actin as well as asymmetric spindle positioning can be blocked by Brefeldin A (BFA) (*17*). BFA treatment did not lead to lagging chromosomes, suggesting that the actin-dependent transport of the spindle and Rab11a-positive vesicles are dispensable for chromosome segregation (Fig. S1C, S5, C, E-F).

We also tested if the failure of cytokinesis in Cytochalasin D-treated and *Fmn2*$^{-/-}$ oocytes contributes to lagging chromosomes (*18, 19*). To this end, we microinjected oocytes with Exoenzyme C3, a specific inhibitor of the small GTPase Rho A that is essential for cytokinesis (*20*) but dispensable for the formation of spindle actin (Fig. S1B). The frequency of lagging chromosomes was not significantly different from BSA injected control oocytes (Fig. 2, H-J, S4, C and F, S5, D and G). Thus, lagging chromosomes in Cytochalasin D-treated and *Fmn2*$^{-/-}$ oocytes are not caused by cytokinetic failure. Collectively, these data establish a role for actin in preventing lagging chromosomes.

Actin drives chromosome alignment during metaphase II

Spindle actin was also present during the second meiotic division (Fig. 1, B and C and movie S10). To investigate the function of spindle actin during meiosis II, we added Cytochalasin D to eggs that had just progressed through anaphase I. Cytochalasin D addition significantly delayed the congression of chromosomes on the metaphase II spindle (Fig. 3, A-C). Consistent with this observation, Cytochalasin D treatment throughout oocyte maturation also caused severe chromosome alignment defects in meiosis II. Instead of being tightly clustered on the metaphase plate, chromosomes were scattered across the entire spindle or trapped at the spindle poles (Fig. 3, D and E, S6, A and B, movies S7 and S9) These defects were independent of actin-mediated vesicle transport as treatment of oocytes with BFA did not have an effect on the efficiency of chromosome alignment (Fig. 3F, S6D).

Cytokinetic failure in Cytochalasin D-treated and *Fmn2*$^{-/-}$ oocytes frequently gave rise to two spindles that later merged into a larger spindle containing twice the number of chromosomes (Fig. S6, G-I, movies S7 and S9). However, misalignment of chromosomes in these eggs was not due to the increased number of chromosomes on their metaphase

II spindles: chromosomes aligned efficiently when cytokinesis was blocked by Exoenyzme C3 or BFA treatment, which led to the same increase in chromosome number without affecting spindle actin (Fig. 3, F and G, S6, C and D).

Strikingly, when we acutely removed actin from metaphase II spindles, accurately aligned chromosomes became displaced from the spindle equator and moved towards the poles, often oscillating between the two spindle poles (Fig. 3, H and I, movies S11 and S12). Thus, actin is required to both align and maintain the correct position of chromosomes on the metaphase II spindle.

Actin prevents lagging chromosomes during anaphase II

Since spindle actin persists during anaphase II (Fig. S7), we investigated if it is also essential for accurate chromosome segregation in meiosis II. Eggs progressed into anaphase II even when chromosomes were trapped at the spindle poles (Fig. 4G), indicating that disruption of actin can indeed give rise to aneuploidy.

The frequency of lagging chromosomes during anaphase II was increased in *Fmn2*$^{-/-}$ eggs (Fig. 4, C and D) and in eggs that had been treated with Cytochalasin D throughout oocyte maturation (Fig. 4, A and B). The increase in lagging chromosomes was not due to cytokinetic failure in these eggs, because blocking cytokinesis by inhibiting Rho A did not lead to lagging chromosomes (Fig. S6, E and F). Chromosome segregation errors in anaphase II were also independent of other previous meiotic defects, because lagging chromosomes were also induced by the acute addition of Cytochalasin D in meiosis II (Fig. 4, E and F). Together, these data suggest that actin is also essential for accurate chromosome segregation during anaphase II.

Mechanism of actin-dependent chromosome alignment and segregation

Why do chromosomes misalign and mis-segregate when actin is disrupted? To address this, we examined if key mechanisms that drive chromosome alignment and segregation are perturbed. The turnover of microtubules in the spindle as well as the flux of microtubules towards the spindle pole, which is thought to promote the movement of chromosomes during anaphase (*21-23*), were not significantly altered (Fig. S8). More

subtle changes in k-fiber dynamics may be masked though by the high abundance of non-kinetochore microtubules in acentrosomal spindles (*24*). Misaligned chromosomes were also positive for MAD1 (Fig. S9), suggesting that they are still recognized by the spindle assembly checkpoint, which monitors the attachment of kinetochores to microtubules (*25*). Notably, the presence of misaligned chromosomes did not block progression of oocytes into anaphase (Fig. 4G) . This is consistent with previous work demonstrating that mouse oocytes progress into anaphase efficiently in the presence of small numbers of misaligned chromosomes (*26-30*).

Actin promotes the formation of kinetochore fibers

K-fibers are instrumental in creating the forces that are required for chromosome segregation (*3, 4*). Thus, we investigated if the formation of k-fibers or their correct interaction with kinetochores relies on spindle actin. To this end, we used a cold-mediated microtubule depolymerization assay, which selectively preserves kinetochore-bound, stable microtubules (k-fibers) (Fig. 5B).

Lagging chromosomes are frequently caused by merotelic microtubule attachments, an incorrect type of kinetochore-microtubule attachment in which a single kinetochore is attached to both spindle poles (Fig. 5A) (*31*). However, the frequency of merotelic attachments was not increased upon disruption of actin (Fig. 5A). Instead, the vast majority of chromosomes was correctly attached to microtubules. Only chromosomes that were trapped at the spindle poles were incorrectly attached, with both kinetochores being either attached to the same spindle pole (syntelic) or one kinetochore being unattached (monotelic) (Fig. 5A).

Next, we assessed if the formation of k-fibers was affected. To measure k-fiber density, we quantified the mean fluorescence intensity of k-fiber isosurface reconstructions that were generated from high resolution three-dimensional image stacks in Imaris (Bitplane) (Fig. 5C). This revealed that the intensity of k-fibers in meiosis I was significantly reduced when actin was absent in *Fmn2*$^{-/-}$ or Cytochalasin D-treated oocytes (Fig. S10, A-D), but not in BFA-treated oocytes (Fig. S10, E and F). Also the acute addition of Cytochalasin D to metaphase II arrested eggs led to a significant reduction in k-fiber intensity (Fig. 5, J

and K). Consistent with these results, treatment of oocytes with Cytochalasin D throughout oocyte maturation reduced the k-fiber intensity of the metaphase II spindle by ~40% (Fig. 5, D and E). This was particularly unexpected because these eggs had twice the number of chromosomes and hence twice the number of kinetochore fibers due to cytokinetic failure. In stark contrast, inhibiting cytokinesis by Exoenzyme C3, which does not affect spindle actin (Fig. S1B), led to a ~1.6 fold increase in k-fiber intensity (Fig. 5, F and G), consistent with an increase in chromosomes on the spindle. *Fmn2*$^{-/-}$ eggs also have twice the number of chromosomes on the spindle but did not show the expected increase in k-fiber intensity (Fig. 5, H and I). Overexpression of the k-fiber dynamics regulating protein CLASP1 (*32*) in *Fmn2*$^{-/-}$ eggs rescued the k-fiber intensity to levels that were similar to those of Exoenzyme C3-microinjected metaphase II eggs (Fig. 5, L and M), providing further evidence that k-fibers are decreased in *Fmn2*$^{-/-}$ eggs. Together, these data suggest that actin promotes the formation of k-fibers in mammalian eggs.

Stabilization of actin leads to chromosome segregation errors

Next, we investigated if actin needs to be dynamic to promote k-fiber formation, chromosome alignment and segregation. To this end, we treated oocytes with high concentrations of SiR-Actin, a derivative of the actin-stabilizing drug Jasplakinolide (Fig. 6A) (*33*). Strikingly, SiR-Actin-treated oocytes were significantly more likely to have chromosome alignment and segregation defects during meiosis I and II (Fig. S6, B and C). High levels of SiR-Actin also blocked cytokinesis and led to the formation of spindles with twice the number of chromosomes. However, the increase in chromosome numbers was not linked to an increase in k-fiber intensity (Fig. S6, D and E), suggesting that actin needs to be dynamic to promote the formation of k-fibers. Consistent with this observation, treatment of oocytes throughout maturation with BFA, which also blocks cytokinesis and vesicle-dependent actin dynamics (*17*), did not lead to an increase in metaphase II k-fiber intensity (Fig. S10, G and H). Together, these data indicate that actin needs to be dynamic to promote k-fiber formation.

Increasing spindle actin enhances k-fiber bundling

How does actin promote the formation of k-fibers? Several *in vivo* and *in vitro* studies suggest that actin can organize, bundle and stabilize microtubules (*34-38*). It was thus conceivable that actin drives the formation of k-fibers by similar mechanisms. The actin filaments in the spindle were on average 1.2±0.4 μm apart (Fig. S11A), suggesting that they are indeed dense enough to bundle and stabilize k-fibers in meiotic spindles.

To test this hypothesis further, we artificially enriched meiotic spindles in actin by targeting the actin-stabilizing calponin-homology (CH) domain of Utrophin to the spindle (Fig. 7B, S11, B and C). The actin-enriched spindles were typically elongated with sharply focused poles, and their microtubules appeared more bundled (Fig. 7, A and B). Cold-mediated microtubule depolymerization revealed a striking increase in the degree of k-fiber bundling in actin-enriched spindles: in the majority of wild-type spindles, k-fibers appeared as individual microtubule bundles (Fig. 7, C-E and S11H). In stark contrast, over 90% of actin-enriched spindles had k-fibers that were not discernible as individual fibers but were instead clustered into thick bundles (Fig. 7, C–D, F and S11I). Also the intensity of k-fibers was significantly increased (Fig. 8, E and F), whereas tubulin turnover and microtubule flux were decreased (Fig. 8, A-D).

While timing and efficiency of anaphase onset were unaffected (Fig. S11, D and E), actin-enriched spindles had gross chromosome alignment and segregation defects (Fig. 8, G-I, movie S13). These defects could be due to excessive bundling of k-fibers (Fig. 7) and reduced turnover and flux of microtubules in these spindles (Fig. 8, A-D). While k-fibers need to be stable enough to pull chromosomes apart during anaphase, they also need to be dynamic enough to allow destabilization of incorrect kinetochore-microtubule attachments (*39-41*). Together, our data establish that reducing or increasing the amount of actin in spindles leads to a decrease or increase in k-fibers, respectively, both of which cause chromosome segregation errors in mammalian eggs.

Discussion

Using a combination of high resolution live cell imaging and loss-of-function assays, we have revealed an unexpected function of actin in segregating chromosomes in

mammalian eggs, a process that is generally thought to be entirely microtubule-dependent. In particular, we found that prominent actin filaments permeate the microtubule spindle in eggs of many mammalian species, including humans. Actin is essential for the accurate alignment and segregation of chromosomes during meiosis (Fig. 8J). Interfering with actin led to a marked increase in lagging chromosomes and a decrease in chromosome speed during anaphase. The lagging chromosomes that were caused by disrupting actin most frequently moved to the correct spindle pole, but sometimes remained in the spindle center (Fig. 4B), where they might be partitioned incorrectly by the cytokinetic furrow. Actin was also essential for the accurate alignment of chromosomes during metaphase II. In many eggs, chromosomes remained located at the spindle poles instead of aligning on the metaphase plate. Despite having severe chromosome alignment defects, these eggs still progressed into anaphase, resulting in aneuploidy.

We report that actin promotes the formation of kinetochore fibers. Our data suggest a model whereby actin helps to bundle and stabilize k-fiber microtubules in the spindle (Fig. 8J). Decreasing or increasing actin in the spindle leads to a reduction or increase in k-fibers, respectively, precluding the accurate alignment and segregation of chromosomes.

Interestingly, chromosome alignment in meiosis I was independent of actin (Fig. S4B). This is consistent with the observation that spindle actin assembles only shortly before anaphase during meiosis I (*14, 15*) whereas the alignment of chromosomes is largely completed several hours before anaphase onset (*42*). The alignment of chromosomes in meiosis I is thus likely to be primarily microtubule- and kinesin-dependent (*42*).

The often slightly weaker phenotypes in *Fmn2*$^{-/-}$ versus Cytochalasin D-treated oocytes may be due to residual actin filaments in the spindles of *Fmn2*$^{-/-}$ eggs (Fig. 1C). These may help to form better functional k-fibers than in Cytochalasin D-treated eggs, where spindle actin is completely disrupted (Fig. 1B).

That actin filaments are required to form k-fibers was unexpected, as k-fibers are generally thought to rely entirely on the cooperative action of microtubule-associated proteins and kinetochore components (*3, 4*). There is extensive evidence though that

actin mediates bundling and organization of microtubules *in vivo* and *in vitro*, consistent with our model (*34-38*). Functionally relevant interactions between actin and microtubules have been reported in various systems to-date (*43*). While our data strongly suggest that the defects in chromosome alignment and segregation are directly due to disrupting spindle actin, it is also still possible that actin promotes alignment and segregation of chromosomes by additional, less direct mechanisms.

Our data add to the emerging picture that actin has many essential functions during meiosis (*44*). For example, spindle positioning, a process that is orchestrated by microtubules in many cell types (*45-47*), is primarily actin-dependent in mouse oocytes (*14, 15, 17, 48*). Actin also mediates the long-range transport of vesicles in mouse oocytes (*16*) and has been implicated in chromosome segregation in grasshopper spermatocytes (*49*). In starfish oocytes, where microtubules are too short to capture chromosomes after nuclear envelope breakdown, a meshwork of contractile actin filaments collects the chromosomes from the large nucleus and delivers them to the assembling spindle (*50*).

The presence of spindle actin in other mammalian eggs, including humans (Fig. S1A), hints at a conserved function in chromosome segregation. This surprising function may even extend beyond mammals, since F-actin has been reported in spindles of a variety of species and cell types (*5, 50-53*).

References and Notes

1. J. P. Welburn *et al.*, The human kinetochore Ska1 complex facilitates microtubule depolymerization-coupled motility. *Developmental cell* **16**, 374-385 (2009).
2. J. C. Schmidt *et al.*, The kinetochore-bound Ska1 complex tracks depolymerizing microtubules and binds to curved protofilaments. *Developmental cell* **23**, 968-980 (2012).
3. H. Maiato, J. DeLuca, E. D. Salmon, W. C. Earnshaw, The dynamic kinetochore-microtubule interface. *Journal of cell science* **117**, 5461-5477 (2004).
4. I. M. Cheeseman, A. Desai, Molecular architecture of the kinetochore-microtubule interface. *Nature reviews. Molecular cell biology* **9**, 33-46 (2008).
5. J. C. Sandquist, A. M. Kita, W. M. Bement, And the dead shall rise: actin and myosin return to the spindle. *Developmental cell* **21**, 410-419 (2011).
6. A. Kuliev, Z. Zlatopolsky, I. Kirillova, J. Spivakova, J. Cieslak Janzen, Meiosis errors in over 20,000 oocytes studied in the practice of preimplantation aneuploidy testing. *Reprod Biomed Online* **22**, 2-8 (2011).

7. A. Kuliev, J. Cieslak, Y. Verlinsky, Frequency and distribution of chromosome abnormalities in human oocytes. *Cytogenet Genome Res* **111**, 193-198 (2005).
8. B. E. Rosenbusch, M. Schneider, Cytogenetic analysis of human oocytes remaining unfertilized after intracytoplasmic sperm injection. *Fertil Steril* **85**, 302-307 (2006).
9. G. A. Brar, A. Amon, Emerging roles for centromeres in meiosis I chromosome segregation. *Nature reviews. Genetics* **9**, 899-910 (2008).
10. T. Chiang, F. E. Duncan, K. Schindler, R. M. Schultz, M. A. Lampson, Evidence that weakened centromere cohesion is a leading cause of age-related aneuploidy in oocytes. *Current biology : CB* **20**, 1522-1528 (2010).
11. S. I. Nagaoka, T. J. Hassold, P. A. Hunt, Human aneuploidy: mechanisms and new insights into an age-old problem. *Nature reviews. Genetics* **13**, 493-504 (2012).
12. T. Hassold, P. Hunt, To err (meiotically) is human: the genesis of human aneuploidy. *Nat Rev Genet* **2**, 280-291 (2001).
13. D. Clift, M. Schuh, Restarting life: fertilization and the transition from meiosis to mitosis. *Nature reviews. Molecular cell biology* **14**, 549-562 (2013).
14. M. Schuh, J. Ellenberg, A new model for asymmetric spindle positioning in mouse oocytes. *Current biology : CB* **18**, 1986-1992 (2008).
15. J. Azoury *et al.*, Spindle positioning in mouse oocytes relies on a dynamic meshwork of actin filaments. *Current biology : CB* **18**, 1514-1519 (2008).
16. M. Schuh, An actin-dependent mechanism for long-range vesicle transport. *Nature cell biology* **13**, 1431-1436 (2011).
17. Z. Holubcova, G. Howard, M. Schuh, Vesicles modulate an actin network for asymmetric spindle positioning. *Nat Cell Biol* **15**, 937-947 (2013).
18. J. Dumont *et al.*, Formin-2 is required for spindle migration and for the late steps of cytokinesis in mouse oocytes. *Dev Biol* **301**, 254-265 (2007).
19. J. Kubiak, A. Paldi, M. Weber, B. Maro, Genetically identical parthenogenetic mouse embryos produced by inhibition of the first meiotic cleavage with cytochalasin D. *Development* **111**, 763-769 (1991).
20. S. Pfender, V. Kuznetsov, S. Pleiser, E. Kerkhoff, M. Schuh, Spire-type actin nucleators cooperate with Formin-2 to drive asymmetric oocyte division. *Current biology : CB* **21**, 955-960 (2011).
21. G. C. Rogers *et al.*, Two mitotic kinesins cooperate to drive sister chromatid separation during anaphase. *Nature* **427**, 364-370 (2004).
22. A. Desai, P. S. Maddox, T. J. Mitchison, E. D. Salmon, Anaphase A chromosome movement and poleward spindle microtubule flux occur At similar rates in Xenopus extract spindles. *The Journal of cell biology* **141**, 703-713 (1998).
23. T. J. Mitchison, E. D. Salmon, Poleward kinetochore fiber movement occurs during both metaphase and anaphase-A in newt lung cell mitosis. *The Journal of cell biology* **119**, 569-582 (1992).
24. R. Ohi, K. Burbank, Q. Liu, T. J. Mitchison, Nonredundant functions of Kinesin-13s during meiotic spindle assembly. *Current biology : CB* **17**, 953-959 (2007).
25. A. Musacchio, E. D. Salmon, The spindle-assembly checkpoint in space and time. *Nat Rev Mol Cell Biol* **8**, 379-393 (2007).
26. A. Kolano, S. Brunet, A. D. Silk, D. W. Cleveland, M. H. Verlhac, Error-prone mammalian female meiosis from silencing the spindle assembly checkpoint

without normal interkinetochore tension. *Proceedings of the National Academy of Sciences of the United States of America* **109**, E1858-1867 (2012).
27. L. Gui, H. Homer, Spindle assembly checkpoint signalling is uncoupled from chromosomal position in mouse oocytes. *Development* **139**, 1941-1946 (2012).
28. S. I. Lane, Y. Yun, K. T. Jones, Timing of anaphase-promoting complex activation in mouse oocytes is predicted by microtubule-kinetochore attachment but not by bivalent alignment or tension. *Development* **139**, 1947-1955 (2012).
29. J. Sebestova, A. Danylevska, L. Novakova, M. Kubelka, M. Anger, Lack of response to unaligned chromosomes in mammalian female gametes. *Cell Cycle* **11**, 3011-3018 (2012).
30. S. I. Nagaoka, C. A. Hodges, D. F. Albertini, P. A. Hunt, Oocyte-specific differences in cell-cycle control create an innate susceptibility to meiotic errors. *Current biology : CB* **21**, 651-657 (2011).
31. J. Gregan, S. Polakova, L. Zhang, I. M. Tolic-Norrelykke, D. Cimini, Merotelic kinetochore attachment: causes and effects. *Trends in cell biology* **21**, 374-381 (2011).
32. H. Maiato *et al.*, Human CLASP1 is an outer kinetochore component that regulates spindle microtubule dynamics. *Cell* **113**, 891-904 (2003).
33. G. Lukinavicius *et al.*, Fluorogenic probes for live-cell imaging of the cytoskeleton. *Nature methods* **11**, 731-733 (2014).
34. E. B. Merriam *et al.*, Synaptic regulation of microtubule dynamics in dendritic spines by calcium, F-actin, and drebrin. *The Journal of neuroscience : the official journal of the Society for Neuroscience* **33**, 16471-16482 (2013).
35. A. W. Schaefer *et al.*, Coordination of actin filament and microtubule dynamics during neurite outgrowth. *Developmental cell* **15**, 146-162 (2008).
36. D. T. Burnette *et al.*, Myosin II activity facilitates microtubule bundling in the neuronal growth cone neck. *Developmental cell* **15**, 163-169 (2008).
37. M. Preciado Lopez *et al.*, Actin-microtubule coordination at growing microtubule ends. *Nature communications* **5**, 4778 (2014).
38. W. Ning *et al.*, The CAMSAP3-ACF7 Complex Couples Noncentrosomal Microtubules with Actin Filaments to Coordinate Their Dynamics. *Developmental cell* **39**, 61-74 (2016).
39. D. Cimini, B. Moree, J. C. Canman, E. D. Salmon, Merotelic kinetochore orientation occurs frequently during early mitosis in mammalian tissue cells and error correction is achieved by two different mechanisms. *Journal of cell science* **116**, 4213-4225 (2003).
40. D. Cimini, X. Wan, C. B. Hirel, E. D. Salmon, Aurora kinase promotes turnover of kinetochore microtubules to reduce chromosome segregation errors. *Current biology : CB* **16**, 1711-1718 (2006).
41. A. E. Kelly, H. Funabiki, Correcting aberrant kinetochore microtubule attachments: an Aurora B-centric view. *Current opinion in cell biology* **21**, 51-58 (2009).
42. T. S. Kitajima, M. Ohsugi, J. Ellenberg, Complete kinetochore tracking reveals error-prone homologous chromosome biorientation in mammalian oocytes. *Cell* **146**, 568-581 (2011).
43. O. C. Rodriguez *et al.*, Conserved microtubule-actin interactions in cell movement and morphogenesis. *Nat Cell Biol* **5**, 599-609 (2003).

44. C. M. Field, P. Lenart, Bulk cytoplasmic actin and its functions in meiosis and mitosis. *Current biology : CB* **21**, R825-830 (2011).
45. C. P. Samora *et al.*, MAP4 and CLASP1 operate as a safety mechanism to maintain a stable spindle position in mitosis. *Nature cell biology* **13**, 1040-1050 (2011).
46. J. A. Knoblich, Mechanisms of asymmetric stem cell division. *Cell* **132**, 583-597 (2008).
47. S. Kotak, P. Gonczy, Mechanisms of spindle positioning: cortical force generators in the limelight. *Current opinion in cell biology* **25**, 741-748 (2013).
48. J. Azoury, K. W. Lee, V. Georget, P. Hikal, M. H. Verlhac, Symmetry breaking in mouse oocytes requires transient F-actin meshwork destabilization. *Development* **138**, 2903-2908 (2011).
49. R. V. Silverman-Gavrila, A. Forer, Evidence that actin and myosin are involved in the poleward flux of tubulin in metaphase kinetochore microtubules of crane-fly spermatocytes. *Journal of cell science* **113 (Pt 4)**, 597-609 (2000).
50. P. Lenart *et al.*, A contractile nuclear actin network drives chromosome congression in oocytes. *Nature* **436**, 812-818 (2005).
51. C. J. Staiger, W. Z. Cande, Microfilament Distribution in Maize Meiotic Mutants Correlates with Microtubule Organization. *The Plant cell* **3**, 637-644 (1991).
52. K. L. Weber, A. M. Sokac, J. S. Berg, R. E. Cheney, W. M. Bement, A microtubule-binding myosin required for nuclear anchoring and spindle assembly. *Nature* **431**, 325-329 (2004).
53. A. Forer, J. D. Pickett-Heaps, Cytochalasin D and latrunculin affect chromosome behaviour during meiosis in crane-fly spermatocytes. *Chromosome Res* **6**, 533-549 (1998).
54. B. Leader *et al.*, Formin-2, polyploidy, hypofertility and positioning of the meiotic spindle in mouse oocytes. *Nat Cell Biol* **4**, 921-928 (2002).
55. M. Schuh, J. Ellenberg, Self-organization of MTOCs replaces centrosome function during acentrosomal spindle assembly in live mouse oocytes. *Cell* **130**, 484-498 (2007).
56. A. Bos-Mikich, K. Swann, D. G. Whittingham, Calcium oscillations and protein synthesis inhibition synergistically activate mouse oocytes. *Molecular reproduction and development* **41**, 84-90 (1995).
57. Z. Holubcova, M. Blayney, K. Elder, M. Schuh, Human oocytes. Error-prone chromosome-mediated spindle assembly favors chromosome segregation defects in human oocytes. *Science* **348**, 1143-1147 (2015).
58. S. L. Byers, S. J. Payson, R. A. Taft, Performance of ten inbred mouse strains following assisted reproductive technologies (ARTs). *Theriogenology* **65**, 1716-1726 (2006).
59. B. Mogessie, D. Roth, Z. Rahil, A. Straube, A novel isoform of MAP4 organises the paraxial microtubule array required for muscle cell differentiation. *eLife* **4**, e05697 (2015).
60. B. M. Burkel, G. von Dassow, W. M. Bement, Versatile fluorescent probes for actin filaments based on the actin-binding domain of utrophin. *Cell motility and the cytoskeleton* **64**, 822-832 (2007).

61. E. D. Salmon, D. A. Begg, Functional implications of cold-stable microtubules in kinetochore fibers of insect spermatocytes during anaphase. *The Journal of cell biology* **85**, 853-865 (1980).

Acknowledgments

We thank the staff of the MRC Laboratory of Molecular Biology's Animal, Genotyping and Microscopy Facilities for technical assistance, and members of the Schuh lab for discussions. We thank Kathleen Scheffler for help with *in vitro* fertilization and mouse embryo imaging experiments. We are thankful to Kay Elder and Martyn Blayney from Bourn Hall Clinic, Cambridge for providing the human oocyte shown in Fig. S1A. We thank Helder Maiato for generously providing a plasmid encoding human CLASP1. Research leading to these results has received financial support from the European Research Council under grant agreement no. 337415.

B.M and M.S. conceived the study, designed the experiments and methods for data analysis; B.M. performed all experiments, analyzed the data and prepared figures; B.M. and M.S. wrote the manuscript; M.S. supervised the study.

The authors declare no competing financial interests.

Supplementary Materials:

Materials and Methods
Fig S1 – S11
References (54-61)
Movies S1 – S13

Materials and Methods

Preparation and microinjection of oocytes

All mice were maintained in a specific pathogen-free environment according to UK Home Office regulations and the guidelines of the MPI-BPC animal facility. Oocytes were isolated from ovaries of 8-12 week old 129 S6/SvEvTac or *Fmn2*$^{-/-}$ mice (*54*), cultured, and microinjected as previously described (*55*). Final concentrations of 48 nM BSA (Sigma) and Exoenzyme C3 (Merck) were calculated by dividing the total amount of injected protein by the total volume of the oocyte. In some experiments, meiotic

progression into anaphase II was induced by activating oocytes with 10 mM $SrCl_2$ in Ca^{2+} free M2 medium (*56*).

Preparation and culturing of the human oocyte shown in Fig. S1A is described in (*57*) and was approved by the UK's National Research Ethics Service under the REC reference 11/EE/0346.

Porcine and ovine ovaries were obtained from a local slaughterhouse and rapidly transported to the laboratory at 37°C in M2 medium. Oocytes covered with several layers of cumulus cells were collected from ovaries by aspiration with an 18-gauge needle and cultured in M2 medium at 37°C for 48 hours prior to fixation and processing.

In vitro fertilization (IVF)

B6CBAF1 female mice were superovulated by injection of pregnant mare serum gonadotropin (PMSG) followed 48 hours later by injection of human chorionic gonadotropin (hCG). 14 hours later meiosis II-arrested eggs were collected from oviducts and IVF was performed in HTF medium (Millipore MR-070-D) as previously described (*58*). After 2-3 hours, zygotes were fixed in anaphase II.

Expression constructs and mRNA synthesis

To mark microtubules, the microtubule binding domain of MAP4 (MAP4-MTBD, 659-1125 aa) was cloned by PCR using primers CAATGTACACCCCGCCAAAC and GTCGACTTAGATGCTTGTCTCC and the full length mouse MAP4 ORF (*59*) as a template. EGFP variant of MAP4-MTBD was generated by inserting the corresponding PCR product into pEGFP-C1 (Clontech). MAD1 was cloned by PCR from mouse cDNA using primers CAAGCTTATGGAAGACCTCGGGG and GAATTCCTAGATAGAGGTCTGGCGGC and inserted into pEGFP-C3 vector (Clontech) to generate a fluorescently-tagged variant. SNAP-tagged MAP4-MTBD was cloned by inserting MAP4-MTBD ORF into pSNAPf (NEB). The coding sequence of human CLASP1 (NM_015282.2) was cloned by PCR using primers GGACTCAGATCTCGAGCTCAATGGAGCCTCGCATGGAG and CCGTCGACTGCAGAATTCGATTAGCTGTGCGTGGAGAC and a pEGFP-CLASP1

(laboratory of Helder Maiato) plasmid as a template. Tagged coding sequences were subsequently inserted into pGEMHE (*55*) for *in vitro* transcription and linearized with AscI. Expression constructs for labelling chromosomes (H2B-mRFP) (*55*) and actin (EGFP-UtrCH) in live cells (*60*) were previously described. EGFP-MAP4-UtrCH was cloned by assembling AgeI-KpnI flanked MAP4-MTBD-2xlinker and KpnI-SalI flanked 2xlinker-UtrCH into the AgeI-SalI site of pGEMHE thereby reconstituting a 4xlinker repetitive nucleotide sequence between MAP4 and UtrCH, each linker encoding amino acids Gly-Gly-Ser. With the exception of Fig. 8, E and F where it was expressed at similar levels to MAP4, EGFP-MAP4-UtrCH in spindle actin enrichment assays was expressed at much lower levels than EGFP-MAP4 (Fig. S11, F and G).

Capped mRNA was synthesized using T7 polymerase (mMessage mMachine kit, following the manufacturer's instructions, Ambion). mRNA concentrations were determined on agarose gels by comparison with an RNA standard (Ambion).

Confocal and super-resolution microscopy

Images were acquired with Zeiss LSM710, LSM780, LSM800 and LSM880 microscopes at 37°C. Oocytes were imaged in M2 medium with or without cytoskeletal inhibitors under mineral oil using a 40x C-Apochromat 1.2 NA water-immersion objective. Super-resolution time-lapse images were acquired using the Airyscan module on Zeiss LSM800 and LSM880 microscopes and processed post-acquisition using ZEN2. For chromosome alignment and segregation analyses, images were typically acquired at a temporal resolution of 5-6 minutes and a spatial resolution of 1.5 µm confocal sections covering ~20 µm.

Manual and automated quantification of misaligned and lagging chromosomes

For analyses of chromosome misalignment in acute drug addition experiments, only chromosomes that became misaligned within two hours after drug treatment were quantified. For analyses of lagging chromosomes, only meiotic spindles that were parallel to the imaging plane were considered. To manually quantify segregation errors, we classified chromosomes that failed to clear the central spindle region within 12 or 18 minutes of anaphase I onset (time 0 refers to last metaphase frame before anaphase

onset) as lagging or severely lagging, respectively (Fig. 2A). Chromosomes that lagged severely were also included in the quantification of mildly lagging chromosomes. Quantification of severely lagging chromosomes exclusively contained those chromosomes that lagged for at least 18 minutes after anaphase onset. Similarly, quantification of mildly misaligned chromosomes as shown in Fig. 2A included chromosomes that were also severely misaligned. To automate the quantification of lagging chromosomes, we reconstructed three-dimensional isosurfaces of fluorescently-labelled chromosomes in Imaris (Bitplane). We then assessed if surfaces other than the two main chromosome masses were detected by the software upon anaphase onset. Surfaces that were detected separately from the two main chromosome masses 12 minutes after the onset of anaphase were scored as lagging. For quantification of chromosome segregation speeds, both lagging and non-lagging chromosomes were analyzed. All quantitative analyses of chromosome alignment defects in meiosis II were performed at least four hours after completion of anaphase I.

Photoactivation experiments

For analyses of microtubule flux and turnover, meiotic spindles that were parallel to the focal plane were selected using H2B-mRFP labelled chromosomes in oocytes co-expressing photoactivatable-GFP (PAGFP)-Tubulin. Line segments were then used to mark regions or interest at least two-thirds or a half-spindle length away from chromosomes. Regions of interest were photoactivated using the 488 nm laser line and images were acquired at an interval of 3 seconds for 2 minutes. Photobleaching not due to microtubule turnover was corrected by monitoring bleaching of a non-activated region outside the spindle. Microtubule flux rates were measured in ImageJ by following the position of intensity maxima in the photoactivated region over time. Microtubule turnover rates were obtained by plotting time versus maximum intensity plots in OriginPro (OriginLab) and fitting single exponential curves to plots thereby determining half-life of fluorescence decay. Single exponential fitting was used because it produced curves with better goodness-of-fit than double exponential fitting.

Immunofluorescence microscopy

Mouse, human, porcine and ovine oocytes were fixed for 25-30 minutes at 37°C with 100 mM HEPES, 50 mM EGTA, 10 mM $MgSO_4$, 2% formaldehyde, and 0.2% Triton X-100 and extracted in PBS supplemented with 0.1% Triton X-100 at 4°C overnight. Antibody, F-actin and chromosome staining were performed for 1-2 hours in PBS, 3% BSA, and 0.1% Triton X-100. Microtubules were stained using primary rat anti-α-tubulin (MCA78S, Serotec; 1:200) and Alexa-Fluor-546- or Alexa-Fluor-647-labelled secondary anti-rat (Molecular Probes 1:200) antibodies. F-actin was stained with Rhodamine phalloidin (Molecular Probes; 1:20). DNA was stained with 5 µg/ml Hoechst 33342 (Molecular Probes).

Images were acquired with Zeiss LSM710, LSM780, LSM800 and LSM880 confocal microscopes equipped with a 63x C-Apochromat 1.2 NA water-immersion objective as previously described (*55*). Images in control and perturbed situations were acquired with identical imaging conditions. Care was taken that images were not saturated during acquisition.

Spindle volume measurements of fixed oocytes were performed in three dimensions using the Isosurface function in Imaris (Bitplane).

Drug addition experiments

To disrupt actin, oocytes were treated with Cytochalasin D (Calbiochem) at a final concentration of 5 µg/ml. To stabilize actin filaments, oocytes were treated with 5 µM SiR-Actin immediately before imaging. To acutely depolymerize microtubules, eggs were treated with 5 µM Nocodazole (Sigma) immediately before imaging. In spindle actin reassembly assays, mouse oocytes expressing fluorescently labelled actin, microtubules and chromosomes were allowed to mature to meiosis II in the presence of Cytochalasin D and washed out into Cytochalasin D free M2 medium immediately before imaging. In acute drug addition experiments, oocytes matured in M2 medium were washed into Cytochalasin D containing M2 medium immediately before imaging. For MII activation of acutely drug-treated eggs, oocytes were incubated with Cytochalasin D for two hours before activation. For chromosome alignment analyses in meiosis II, acute drug additions

were performed more than four hours after completion of anaphase I. To inhibit vesicle biogenesis, oocytes were treated with 10 μM BFA (Brefeldin A, Sigma).

Cold-mediated microtubule depolymerization assays

To determine k-fiber stability, a previously described assay for specific depolymerization of non-kinetochore associated microtubules was adapted (*61*). Briefly, non-kinetochore microtubules were depolymerized by placing oocyte containing culture dishes at 4°C for 15 minutes. Cells were immediately fixed following cold treatment and processed for immunofluorescence microscopy as described above. k-fiber fluorescence intensities were measured from three-dimensional isosurface reconstructions of spindles using Imaris (Bitplane).

Statistics

Average (mean), standard error of the mean, standard deviation and statistical significance based on two-tailed Student's t test or Fisher's exact test were calculated in OriginPro (OriginLab). *p* values are designated as * for $p < 0.05$, ** for $p < 0.005$ and *** for $p < 0.0005$. Non-significant values are indicated as N.S.

Figure Legends

Fig. 1 Actin filaments permeate the microtubule spindle during anaphase in mouse oocytes.

(**A**) Stills from a single confocal section time lapse movie showing spindle actin (EGFP-UtrCH, grey) and chromosomes (H2B-mRFP, magenta) during anaphase I in a mouse oocyte.

(**B-C**) Single confocal section images of phalloidin stained spindle actin in DMSO- or Cytochalasin D-treated (CytoD) (B) and *Fmn2*$^{+/+}$ or *Fmn2*$^{-/-}$ (C) eggs. Actin (phalloidin) is shown in grey and chromosomes (Hoechst) are shown in magenta. Scale bars, 10 μm.

Fig. 2 Disruption of F-actin causes lagging chromosomes during anaphase I.

(**A**) Scheme illustrating the criteria that were used to quantify mild and severely lagging chromosomes and chromosome misalignment in live mouse oocytes.
(**B**) Frequency of mildly lagging chromosomes in DMSO- or Cytochalasin D-treated oocytes quantified as in A. Data are from 9 independent experiments.

(**C**) Chromosome segregation speeds in DMSO- or Cytochalasin D-treated oocytes. Data are from 3 independent experiments.

(**D**) Stills from representative time lapse movies of anaphase I in DMSO- or Cytochalasin D-treated oocytes. Microtubules (EGFP-MAP4-MTBD) are shown in grey and chromosomes (H2B-mRFP) are shown in magenta. Dashed line boxes mark regions that are magnified in insets.

(**E**) Frequency of mildly lagging chromosomes in *Fmn2*$^{+/+}$ or *Fmn2*$^{-/-}$ oocytes quantified as in A. Data are from 7 independent experiments.

(**F**) Chromosome segregation speeds in *Fmn2*$^{+/+}$ or *Fmn2*$^{-/-}$ oocytes. Data are from 3 independent experiments.

(**G**) Maximum intensity projection stills from representative time lapse movies of anaphase I in *Fmn2*$^{+/+}$ or *Fmn2*$^{-/-}$ oocytes. Microtubules (EGFP-MAP4-MTBD) are shown in grey and chromosomes (H2B-mRFP) are shown in magenta. Dashed line boxes mark regions that are magnified in insets.

(**H**) Frequency of mildly lagging chromosomes in BSA- or Exoenzyme C3-microinjected oocytes quantified as in A. Data are from 3 independent experiments.

(**I**) Chromosome segregation speeds in BSA- or Exoenzyme C3-microinjected oocytes. Data are from 3 independent experiments.

(**J**) Maximum intensity projection stills from representative time lapse movies of anaphase I in BSA- or Exoenzyme C3-microinjected oocytes. Microtubules (EGFP-MAP4-MTBD) are shown in grey and chromosomes (H2B-mRFP) are shown in magenta. Dashed line boxes mark regions that are magnified in insets. Scale bars, 10 μm. Error bars represent S.E.M. Box plots show median (horizontal white lines), mean (small white squares), 25th and 75th percentiles (boxes), 5th and 95th percentiles (whiskers), and, where present, outliers (small lines). The number of analyzed oocytes is specified in italics. Fisher's exact test was used to test for significance in B, E and H. Two-tailed Student's t test was used to test for significance in C, F and I. Z-projections: 16 sections every 1.5 μm.

Fig. 3 Actin promotes chromosome alignment during metaphase II.

(**A**) Stills from representative time lapse movies of chromosome congression in DMSO- or Cytochalasin D-treated mouse eggs. Eggs were treated with DMSO or Cytochalasin D after completion of anaphase I. Microtubules (EGFP-MAP4-MTBD) are shown in grey and chromosomes (H2B-mRFP) are shown in magenta.

(**B**) Quantification of chromosome congression on the metaphase II spindle in eggs treated with DMSO or Cytochalasin D after completion of anaphase I.

(**C**) Average time of chromosome congression in DMSO- or Cytochalasin D-treated eggs.

(**D-G**) Representative images and frequency of severe chromosome misalignment in DMSO- or Cytochalasin D-treated (D), *Fmn2*$^{+/+}$ or *Fmn2*$^{-/-}$ (E), MeOH- or BFA-treated (F)

and BSA- or Exoenzyme C3-microinjected (G) eggs. Microtubules (EGFP-MAP4-MTBD) are shown in grey and chromosomes (H2B-mRFP) are shown in magenta. Arrowheads highlight severely misaligned chromosomes.

(**H**) Frequency of severe chromosome misalignment in eggs that were acutely treated with DMSO or Cytochalasin D.

(**I**) Stills from representative time lapse movies of chromosome misalignment in acutely DMSO- or Cytochalasin D-treated eggs. Dashed line boxes mark regions that are magnified in insets. Microtubules (EGFP-MAP4-MTBD) are shown in grey and chromosomes (H2B-mRFP) are shown in magenta. Scale bar, 10 μm.

Error bars represent S.E.M. Data are from 2 (B and C), 4 (D-F) and 3 (G-H) independent experiments. The number of analyzed eggs is specified in italics. Chromosome misalignment was quantified as in Fig. 2A. Fisher's exact test was used to test for significance. Z-projections: 16 sections every 1.5 μm.

Fig. 4 Disruption of F-actin causes lagging chromosomes during anaphase II.

(**A**) Frequency of lagging chromosomes in DMSO- or Cytochalasin D-treated eggs quantified as in Fig. 2A. Data are from 5 independent experiments.

(**B**) Stills from representative time lapse movies of anaphase II in DMSO- or Cytochalasin D-treated eggs. Dashed line boxes mark regions that are magnified in insets. Microtubules (EGFP-MAP4-MTBD) are shown in grey and chromosomes (H2B-mRFP) are shown in magenta.

(**C**) Frequency of lagging chromosomes in *Fmn2*$^{+/+}$ or *Fmn2*$^{-/-}$ eggs quantified as in Fig. 2A. Data are from 4 independent experiments.

(**D**) Stills from representative time lapse movies of anaphase II in *Fmn2*$^{+/+}$ or *Fmn2*$^{-/-}$ eggs. Dashed line boxes mark regions that are magnified in insets. Microtubules (EGFP-MAP4-MTBD) are shown in grey and chromosomes (H2B-mRFP) are shown in magenta.

(**E**) Frequency of lagging chromosomes in eggs acutely treated with DMSO or Cytochalasin D quantified as in Fig. 2A. Data are from 3 independent experiments.

(**F**) Stills from representative time lapse movies of anaphase II in eggs acutely treated with DMSO or Cytochalasin D. Dashed line boxes mark regions that are magnified in insets. Microtubules (EGFP-MAP4-MTBD) are shown in grey and chromosomes (H2B-mRFP) are shown in magenta.

(**G**) Frequency of DMSO- or Cytochalasin D-treated and *Fmn2*$^{+/+}$ or *Fmn2*$^{-/-}$ eggs with chromosomes trapped at spindle poles at anaphase II onset. Data are from 4 independent experiments. Scale bars, 10 μm. Error bars represent S.E.M. The number of analyzed eggs is specified in italics. Fisher's exact test was used to test for significance. Z-projections: 16 sections every 1.5 μm.

Fig. 5 Actin promotes the formation of kinetochore fibers.

(**A**) Quantification of monotelic (only one kinetochore is attached to microtubules), merotelic (a single kinetochore is attached to k-fibers originating from both spindle poles) and syntelic (both kinetochores are attached to k-fibers originating from the same spindle pole) kinetochore-microtubule attachments in DMSO- or Cytochalasin D-treated eggs.

(**B-C**) To investigate if disruption of actin perturbs the formation of k-fibers, we selectively depolymerized the more dynamic, non-kinetochore-bound microtubules by briefly placing the oocytes on ice (B). We then fixed the cold-treated oocytes and immunostained the remaining population of kinetochore-bound, stable microtubules (k-fibers) with an antibody against α-tubulin (B). As a measure of k-fiber density, we quantified the mean fluorescence intensities of three-dimensional isosurface reconstructions of k-fibers that were generated from high spatial resolution images using Imaris (Bitplane) (C, isosurface reconstruction).

(**D**) Representative immunofluorescence images of k-fibers in DMSO- or Cytochalasin D-treated eggs. Microtubules (tubulin) are shown in grey and chromosomes (Hoechst) are shown in magenta. Insets are magnifications of regions marked by dashed line boxes.

(**E**) Quantification of normalized fluorescence intensity of k-fibers in DMSO- or Cytochalasin D-treated eggs.

(**F-M**) Representative immunofluorescence images of k-fibers and normalized fluorescence intensity quantifications in BSA- or Exoenzyme C3-microinjected (F and G) *Fmn2*$^{+/+}$ or *Fmn2*$^{-/-}$ (H and I), acutely DMSO- or Cytochalasin D-treated (J and K) and CLASP1 expressing *Fmn2*$^{+/+}$ or *Fmn2*$^{-/-}$ eggs (L and M). Microtubules (tubulin) are shown in grey and chromosomes (Hoechst) are shown in magenta. Scale bars, 10 µm. Box plots are as described in Fig. 2. Data are from 3 (A, E, I, K and M) and 2 (G) independent experiments. The number of analyzed oocytes is specified in italics. Two-tailed Student's t test was used to test for significance. Z-projections: 20 sections every 1.5 µm.

Fig. 6 Stabilization of actin by jasplakinolide leads to chromosome alignment and segregation errors.

(**A**) Spindle actin in a live mouse egg labelled with SiR-Actin, a derivative of the actin-stabilizing drug Jasplakinolide.

(**B**) Frequency of mildly lagging chromosomes during anaphase I in DMSO- or SiR-Actin-treated oocytes. Data are from 3 independent experiments.

(**C**) Representative images and frequency of severe chromosome misalignment in DMSO- or SiR-Actin-treated eggs. Arrowheads indicate severely misaligned chromosomes. Scale bar, 10 μm. Data are from 3 independent experiments. Z-projections: 16 sections every 1.5 μm

(**D**) Representative immunofluorescence images of k-fibers (tubulin, grey) and chromosomes (Hoechst, magenta) in DMSO- or SiR-Actin-treated eggs. Insets are magnifications of regions marked by dashed line boxes. Z-projections: 20 sections every 1.5 μm.

(**E**) Quantification of normalized fluorescence intensity of k-fibers in DMSO- or SiR-Actin-treated eggs. Data are from 3 independent experiments. Error bars represent S.E.M. Box plots are as described in Fig. 2. The number of analyzed oocytes is specified in italics. Fisher’s exact test (B-C) and two-tailed Student's t test (E) were used to test for significance.

Fig. 7 Increasing spindle actin enhances k-fiber bundling

(**A**) Microtubule bundling and spindle pole organization in control (MAP4) and actin-enriched (MAP4-UtrCH) spindles. Microtubules are shown in grey and chromosomes (H2B-mRFP) are shown in magenta. Insets are 5x magnifications of dashed boxes.

(**B**) Representative phalloidin staining of actin in control and actin-enriched spindles presented as overexposed (with visible cytoplasmic network) and non-overexposed (bottom panel) images. Actin (phalloidin) is shown in grey and chromosomes (Hoechst) are shown in magenta.

(**C**) Categories for quantification of individualized or bundled microtubules.

(**D**) Quantification of K-fiber bundling in control or actin-enriched meiosis II spindles using categories shown in C. Data are from 3 independent experiments. Error bars represent S.E.M. The number of analyzed eggs is specified in italics. Fisher's exact test was used to test for significance.

(**E-F**) EGFP fluorescence profile analyses of k-fiber bundling in control (E) and actin-enriched (F) spindles. ImageJ was used to obtain the fluorescence profile of lines (shown in white) that were drawn perpendicularly to the long axes of spindles at the indicated positions. Scale bars, 10 μm. Z-projections: 16 sections every 1.5 μm (A and B).

Fig. 8 Increasing spindle actin affects microtubule dynamics and leads to lagging and misaligned chromosomes

(**A**) Rate of microtubule flux (quantified as shown in Fig. S8A) in control (MAP4) or actin-enriched (MAP4-UtrCH) spindles. Data are from 3 independent experiments.

(**B**) Half-life of fluorescence signal dissipation (quantified as shown in Fig. S8A) in control (MAP4) or actin-enriched (MAP4-UtrCH) spindles. Data are from 3 independent experiments.

(**C**) Distribution of half-life of fluorescence signal dissipation values in control (MAP4) or actin-enriched (MAP4-UtrCH) spindles. Data are from 3 independent experiments.

(**D**) Representative single section confocal stills from time lapse movies of tubulin photoactivation in control (MAP4) or actin-enriched (MAP4-UtrCH) spindles.

(**E**) Representative immunofluorescence images of k-fibers in control or actin-enriched meiosis II spindles. Microtubules (tubulin) are shown in grey and chromosomes (Hoechst) are shown in magenta. Insets are magnifications of regions marked by dashed line boxes. Z-projections: 20 sections every 1.5 µm

(**F**) Quantification of normalized fluorescence intensity of k-fibers in control or actin-enriched spindles. Data are from 3 independent experiments.

(**G**) Stills from representative time lapse movies of anaphase I in oocytes expressing MAP4 or MAP4-UtrCH. Microtubules are shown in grey and chromosomes (H2B-mRFP) are shown in magenta. Z-projections: 16 sections every 1.5 µm.

(**H**) Frequency of mildly lagging chromosomes in oocytes expressing MAP4 or MAP4-UtrCH quantified as in Fig. 2A. Data are from 3 independent experiments.

(**I**) Frequency of misaligned chromosomes in eggs expressing MAP4 or MAP4-UtrCH quantified as in Fig. 2A. Data are from 3 independent experiments.

(**J**) Model for the function of actin in protecting eggs against aneuploidy. Bundling of microtubules into functional k-fibers by actin promotes correct alignment of chromosomes in metaphase and their accurate segregation during anaphase. Disruption of actin compromises k-fibers and leads to chromosome alignment and segregation defects, and subsequently to aneuploidy. Scale bars, 10 μm. Error bars represent S.E.M. Box plots are as described in Fig. 2. The number of analyzed oocytes is specified in italics. Two-tailed Student's t test (A, C and F) and Fisher's exact test (H and I) were used to test for significance.

Fig. S1 Actin filaments permeate the microtubule spindle in many mammalian oocytes, including humans.

(**A**) Single confocal section images of spindle actin (phalloidin, grey) and chromosomes (Hoechst, magenta) in fixed mouse, human, porcine and ovine eggs.

(**B-C**) Single confocal section images of phalloidin stained spindle actin in BSA- or Exoenzyme C3-microinjected (B) and MeOH- or BFA-treated (C) eggs. Actin (phalloidin) is shown in grey and chromosomes (Hoechst) are shown in magenta. Scale bars, 10 μm.

Fig. S2 Spindle actin is assembled from the cytoplasmic actin network and is microtubule-dependent.

(**A**) To determine the origin of actin filaments in the spindle, we first depolymerized actin with Cytochalasin D and then washed out the drug so that actin filaments could regrow. We then performed simultaneous super-resolution live imaging of actin, microtubules and chromosomes to investigate how spindle actin reassembles. When regrowth ensued, filaments from the actin network that fills the cytoplasm of mouse oocytes were pulled into and aligned with the microtubule spindle. Panels show stills from single section super-resolution (Zeiss Airyscan), three-color time lapse movies of actin filament recruitment into the meiosis II spindle after Cytochalasin D washout. Arrowheads indicate recruitment of filaments by pulling (upper panel) and alignment (lower panel) events. Scale bar, 5 μm. Actin (EGFP-UtrCH) is shown in green, microtubules (SNAP-M4-MTBD) are shown in grey and chromosomes (H2B-mRFP) are shown in magenta.

(**B**) Stills from single section super-resolution (Zeiss Airyscan) movie of microtubules, actin and chromosomes in a mouse egg during microtubule depolymerization. Microtubules were depolymerized by the addition of Nocodazole after assembly of the spindle in meiosis II. Actin (EGFP-UtrCH) is shown in green, microtubules (SNAP-M4-MTBD) are shown in grey and chromosomes (H2B-mRFP) are shown in magenta. Actin filaments disappeared concomitantly with microtubules after drug addition. Scale bar, 5 μm.

Fig. S3 Spindle actin is disrupted by Cytochalasin D

(**A-B**) Stills from single section super-resolution (Zeiss Airyscan) time lapse movies of microtubules (SNAP-MAP4-MTBD, grey), actin (EGFP-UtrCH, green) and chromosomes (H2B-mRFP, magenta) during anaphase I in DMSO-treated (A) or Cytochalasin D-treated (B) oocytes. Scale bars, 10 μm.

Fig. S4 Actin is not required for general progression through meiosis.

(**A**) Time from nuclear envelope breakdown (NEBD) to anaphase I onset in DMSO- or Cytochalasin D-treated and *Fmn2*$^{+/+}$ or *Fmn2*$^{-/-}$ oocytes. Data are from 3 independent experiments.

(**B**) Frequency of chromosome misalignment in DMSO- or Cytochalasin D-treated (5 independent experiments) and *Fmn2*$^{+/+}$ or *Fmn2*$^{-/-}$ (7 independent experiments) meiosis I oocytes.

(**C**) Efficiency of anaphase I onset in DMSO- or Cytochalasin D-treated, *Fmn2*$^{+/+}$ or *Fmn2*$^{-/-}$ and BSA- or Exoenzyme C3-microinjected oocytes. Data are from 3 independent experiments.

(**D**) Measurements of anaphase I spindle elongation in DMSO- or Cytochalasin D-treated live oocytes. Spindle length at 0 min is measured one time point before anaphase I onset in 6 min time lapse movies. Data are from 4 independent experiments.

(**E**) Measurements (as described in D) of anaphase I spindle elongation in *Fmn2*$^{+/+}$ or *Fmn2*$^{-/-}$ live oocytes. Data are from 4 independent experiments.

(**F**) Measurements (as described in D) of anaphase I spindle elongation in BSA- or Exoenzyme C3-microinjected live oocytes. Data are from 3 independent experiments. Error bars represent S.E.M. Box plots are as described in Fig. 2. The number of analyzed oocytes is specified in italics. Fisher's exact test (B and C) and two-tailed Student's t test (A, D-F) were used to test for significance.

Fig. S5 Disrupting actin-mediated vesicle transport or cytokinesis does not lead to lagging chromosomes.

(**A-D**) Frequency of severely lagging chromosomes in DMSO- or Cytochalasin D-treated (A, 9 independent experiments), *Fmn2*$^{+/+}$ or *Fmn2*$^{-/-}$ (B, 7 independent experiments), MeOH- or BFA-treated (C, 4 independent experiments) and BSA- or Exoenzyme C3-microinjected (D, 3 independent experiments) meiosis I oocytes quantified as in Fig. 2A.
(**E**) Frequency of mildly lagging chromosomes in MeOH- or BFA-treated meiosis I oocytes quantified as in Fig. 2A. Data are from 4 independent experiments.
(**F**) Stills from representative time lapse movies of anaphase I in MeOH- or BFA-treated oocytes. Scale bar, 10 µm. Microtubules (EGFP-MAP4-MTBD) are shown in grey and chromosomes (H2B-mRFP) are shown in magenta. Z-projections: 16 sections every 1.5 µm.

(**G**) Quantification of mildly lagging chromosomes by automated identification chromosomes (as defined in schematics in Fig. 2A) in DMSO- or Cytochalasin D-treated (4 independent experiments), *Fmn2*$^{+/+}$ or *Fmn2*$^{-/-}$ (7 independent experiments) and BSA- or Exoenzyme C3-microinjected (3 independent experiments) meiosis I oocytes.

(**H**) Automated identification of lagging chromosomes (upper panel) by three-dimensional isosurface reconstruction (lower panel) of H2B-mRFP fluorescence signal. Arrowheads indicate lagging chromosome. Error bars represent S.E.M. The number of analyzed oocytes is specified in italics. Box plots are as described in Fig. 2. Z-projections: 16 sections every 1.5 µm. Fisher's exact test was used to test for significance.

Fig. S6 Actin is required for chromosome alignment in meiosis II.

(**A-D**) Frequency of mildly misaligned chromosomes (quantified as in Fig. 2A) in DMSO- or Cytochalasin D-treated (A, 7 independent experiments), *Fmn2*$^{+/+}$ or *Fmn2*$^{-/-}$ (B, 7 independent experiments), BSA- or Exoenzyme C3-microinjected oocytes (C, 3 independent experiments) and MeOH- or BFA-treated (D, 10 independent experiments) eggs.

(**E**) Frequency of lagging chromosomes in BSA- or Exoenzyme C3-microinjected eggs quantified as in Fig. 2A. Data are from 3 independent experiments.

(**F**) Stills from representative time lapse movies of anaphase II in BSA- or Exoenzyme C3-microinjected eggs. Microtubules (EGFP-MAP4-MTBD) are shown in grey and chromosomes (H2B-mRFP) are shown in magenta. Scale bars, 10 µm. Z-projections: 16 sections every 1.5 µm.

(**G**) Three-dimensional isosurface reconstruction (lower panel) of microtubules from immunofluorescence images (upper panel) for quantification of meiotic spindle volume.

(**H-I**) Metaphase II spindle volumes in DMSO- or Cytochalasin D-treated (H) and *Fmn2*$^{+/+}$ or *Fmn2*$^{-/-}$ (I) eggs. Data are from 3 independent experiments.

(**J-K**) Meiosis II bipolar spindle lengths in DMSO- or Cytochalasin D-treated (J) and *Fmn2*$^{+/+}$ or *Fmn2*$^{-/-}$ (K) eggs. Data are from 3 independent experiments.

(**L**) Metaphase II spindle volumes in acutely DMSO- or Cytochalasin D-treated eggs. N = 3 independent experiments. Error bars represent S.E.M. Box plots are as described in Fig. 2. The number of analyzed oocytes is specified in italics. Fisher's exact test (A-E) and two-tailed Student's t test (H-L) were used to test for significance.

Fig. S7 Spindle actin is present during anaphase II.

(**A**) Stills from a single confocal section time lapse movie of spindle actin (EGFP-UtrCH, grey) and chromosomes (H2B-RFP, magenta) during anaphase II in a mouse egg.

(**B**) Phalloidin stained spindle actin (grey) and chromosomes (Hoechst, magenta) in an *in vitro* fertilized mouse zygote progressing through anaphase II. Single confocal sections spaced 1.5 μm apart are shown. Scale bars, 10 μm.

Fig. S8 F-actin disruption does not alter microtubule flux or turnover

(**A**) Schematics and stills from photoactivation of spindle microtubules in a control egg. Green line is used for construction of a kymograph to demonstrate movement of photoactivation signal over time due to microtubule flux. Schematics of signal dissipation demonstrate loss of fluorescence signal due to microtubule turnover.

(**B**) Rate of microtubule flux in DMSO- or Cytochalasin D-treated eggs. Data are from 4 independent experiments.

(**C**) Half-life of fluorescence signal dissipation in DMSO- or Cytochalasin D-treated eggs. Data are from 4 independent experiments.

(**D**) Distribution of half-life of fluorescence signal dissipation values in DMSO- or Cytochalasin D-treated eggs. Error bars represent S.E.M. Box plots are as described in Fig. 2. The number of analyzed oocytes is specified in italics. Two-tailed Student's t test was used to test for significance.

Fig. S9 Misaligned chromosomes in eggs lacking F-actin are positive for MAD1

Stills from representative time lapse movies showing chromosomes (H2B-mRFP, magenta) and kinetochore localization of MAD1 (green) in oocytes treated with DMSO or Cytochalasin D throughout maturation. Insets show magnifications of dashed line boxes. Scale bar, 10 μm. 36/40 misaligned chromosomes in Cytochalasin D-treated oocytes were MAD1-positive. 48 oocytes from 6 independent experiments were analyzed. Z-projections: 16 sections every 1.5 μm.

Fig. S10 Actin promotes the formation of k-fibers in meiosis I.

(**A**) Representative immunofluorescence images of k-fibers (tubulin) and chromosomes (Hoechst) in DMSO- or Cytochalasin D-treated meiosis I oocytes. Magnified insets are of spindle regions marked by dashed line boxes.

(**B**) Quantification of normalized fluorescence intensity of k-fibers in DMSO- or Cytochalasin D-treated meiosis I oocytes.

(**C-F**) Representative immunofluorescence images of k-fibers (tubulin) and chromosomes (Hoechst), and normalized fluorescence intensity quantifications in *Fmn2*$^{+/+}$ or *Fmn2*$^{-/-}$ (C and D) and MeOH- or BFA-treated (E and F) meiosis I oocytes. Magnified insets are of spindle regions marked by dashed line boxes.

(**G**) Representative immunofluorescence images of k-fibers (tubulin) and chromosomes (Hoechst) in MeOH- or BFA-treated eggs. Magnified insets are of spindle regions marked by dashed line boxes.

(**H**) Quantification of normalized fluorescence intensity of k-fibers in MeOH- or BFA-treated eggs. Scale bars, 10 μm. Box plots are as described in Fig. 2. Data are from 2 independent experiments in B and F, and 3 independent experiments in D and H. The number of analyzed oocytes is specified in italics. Two-tailed Student's t test was used to test for significance. Z-projections: 20 sections every 1.5 μm.

Fig. S11 Increasing spindle actin promotes k-fiber bundling

(**A**) Distance between neighboring actin filaments within meiosis II spindles. Data are from 4 independent experiments.

(**B**) Phalloidin staining of spindle actin and the actin network in meiosis II. Magnified insets are of regions in the spindle ($I_{spindle}$) and the cytoplasmic network ($I_{network}$) marked by dashed line boxes. Scale bar, 10 μm.

(**C**) Targeting the calponin-homology (CH) domain of Utrophin to the spindle stabilizes actin filaments inside the spindle without affecting the density of the cytoplasmic actin network. Box plots show the distribution of ratios of spindle actin mean fluorescence intensity ($I_{spindle}$) to cytoplasmic actin network mean fluorescence intensity ($I_{network}$) in MAP4 or MAP4-UtrCH expressing eggs. Data are from 3 independent experiments.

(**D**) Time from nuclear envelope breakdown (NEBD) to anaphase I onset in MAP4 or MAP4-UtrCH expressing oocytes. Data are from 3 independent experiments.

(**E**) Efficiency of anaphase I onset in MAP4 or MAP4-UtrCH expressing oocytes. Data are from 3 independent experiments.

(**F**) Quantification of expression levels using normalized EGFP fluorescence intensity inside the spindles of EGFP-MAP4 or EGFP-MAP4-UtrCH expressing eggs. Data are from 3 independent experiments.

(**G**) Quantification of normalized fluorescence intensity of k-fibers in control oocytes expressing MAP4 or oocytes expressing very low levels of MAP4-UtrCH (as quantified in F). Data are from 3 independent experiments.

(**H-I**) EGFP fluorescence profile analyses of k-fiber bundling in control (H) and actin-enriched (I) spindles. ImageJ was used to obtain the fluorescence profile of lines (shown in white) that were drawn perpendicularly to the long axes of spindles at the indicated positions. Error bars represent S.E.M. Box plots are as described in Fig. 2. The number of analyzed oocytes is specified in italics. Fisher's exact test (E) and two-tailed Student's t test (A, C-D, F-G) were used to test for significance.

Supplementary Movies

Movie S1 Time lapse movie of spindle actin during anaphase I in a mouse oocyte microinjected with EGFP-UtrCH (to label actin) and H2B-mRFP (to label chromosomes)

Movie S2 Time lapse movie of spindle actin during meiosis I spindle relocation in a mouse oocyte microinjected with EGFP-UtrCH (to label actin) and H2B-mRFP (to label chromosomes)

Movie S3 Super-resolution (Zeiss Airyscan) time lapse movie of spindle microtubule depolymerization by Nocodazole in a mouse egg. SNAP-MAP4-MTBD (to label microtubules) in grey, H2B-mRFP (to label chromosomes) in magenta and EGFP-UtrCH (to label actin) in green are shown.

Movie S4 Super-resolution (Zeiss Airyscan) time lapse movie of spindle actin during anaphase I in a DMSO-treated oocyte. SNAP-MAP4-MTBD (to label microtubules) in grey, H2B-mRFP (to label chromosomes) in magenta and EGFP-UtrCH (to label actin) in green are shown.

Movie S5 Super-resolution (Zeiss Airyscan) time lapse movie of spindle actin during anaphase I in a Cytochalasin D-treated oocyte. SNAP-MAP4-MTBD (to label microtubules) in grey, H2B-mRFP (to label chromosomes) in magenta and EGFP-UtrCH (to label actin) in green are shown.

Movie S6 Time lapse movie of meiotic maturation of a DMSO-treated mouse oocyte expressing EGFP-MAP4-MTBD (to label microtubules) and H2B-mRFP (to label chromosomes)

Movie S7 Time lapse movie of meiotic maturation of a Cytochalasin D-treated mouse oocyte expressing EGFP-MAP4-MTBD (to label microtubules) and H2B-mRFP (to label chromosomes)

Movie S8 Time lapse movie of meiotic maturation of a *Fmn2*$^{+/+}$ mouse oocyte expressing EGFP-MAP4-MTBD (to label microtubules) and H2B-mRFP (to label chromosomes)

Movie S9 Time lapse movie of meiotic maturation of *Fmn2*$^{-/-}$ mouse oocyte expressing EGFP-MAP4-MTBD (to label microtubules) and H2B-mRFP (to label chromosomes)

Movie S10 Super-resolution (Zeiss Airyscan) time lapse movie of actin, microtubules and chromosomes in a meiosis II mouse oocyte expressing EGFP-UtrCH (to label actin), SNAP-MAP4-MTBD (to label microtubules) and H2B-mRFP (to label chromosomes)

Movie S11 Time lapse movie of microtubules (labelled with EGFP-MAP4-MTBD) and chromosomes (labelled with H2B-mRFP) in a mouse oocyte acutely treated with DMSO in meiosis II

Movie S12 Time lapse movie of microtubules (labelled with EGFP-MAP4-MTBD) and chromosomes (labelled with H2B-mRFP) in a mouse oocyte acutely treated with Cytochalasin D in meiosis II

Movie S13 Time lapse movie showing chromosome misalignment and mis-segregation in a mouse oocyte expressing H2B-mRFP (to labels chromosomes) and EGFP-MAP4-UtrCH (to enrich spindle actin).

Fig. 1

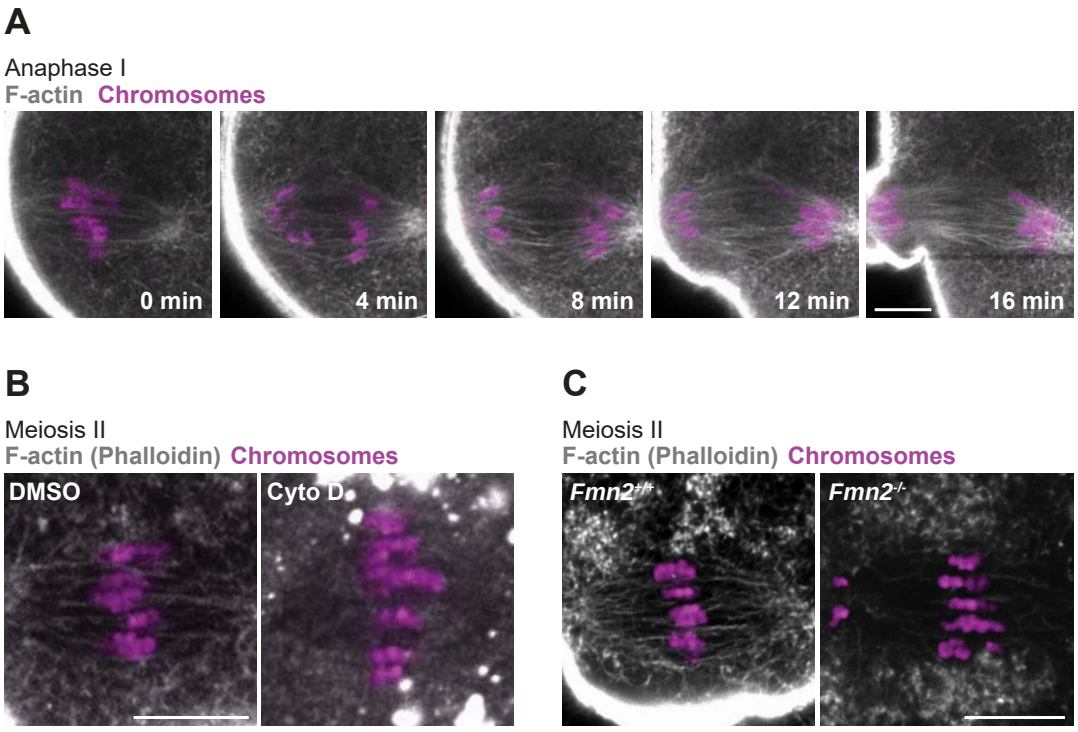
A
Anaphase I
F-actin Chromosomes
0 min
4 min
8 min
12 min
16 min
B
Meiosis II
F-actin (Phalloidin) Chromosomes
DMSO
Cyto D
C
Meiosis II
F-actin (Phalloidin) Chromosomes
Fmn2+/+
Fmn2-/-

Fig. 2

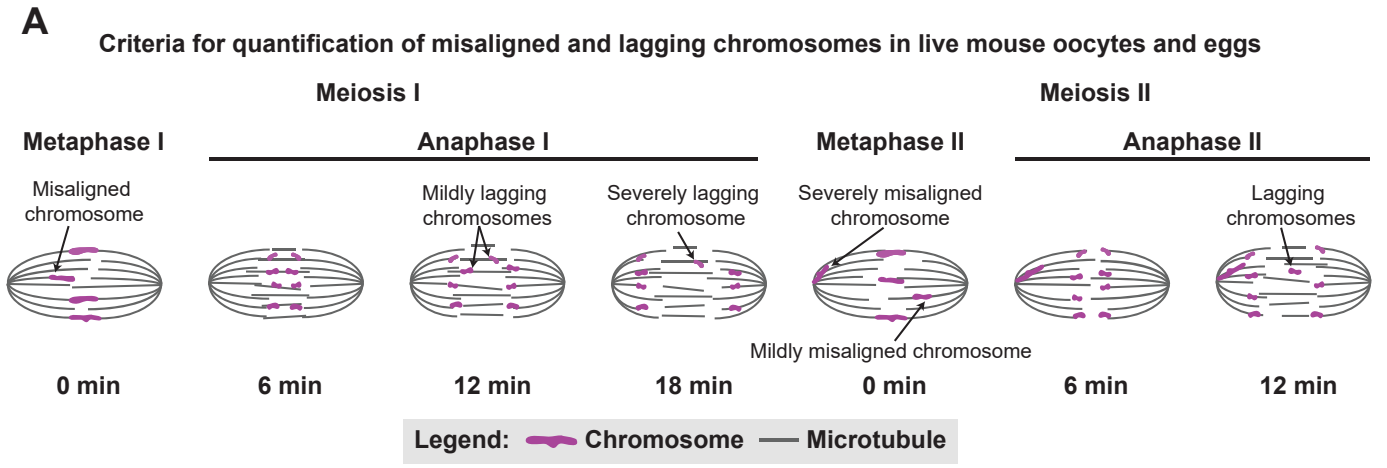
A
Criteria for quantification of misaligned and lagging chromosomes in live mouse oocytes and eggs
Meiosis I
Meiosis II
Metaphase I
Anaphase I
Metaphase II
Anaphase II
Misaligned chromosome
Mildly lagging chromosomes
Severely lagging chromosome
Severely misaligned chromosome
Lagging chromosomes
Mildly misaligned chromosome
0 min
6 min
12 min
18 min
0 min
6 min
12 min
Legend: Chromosome Microtubule

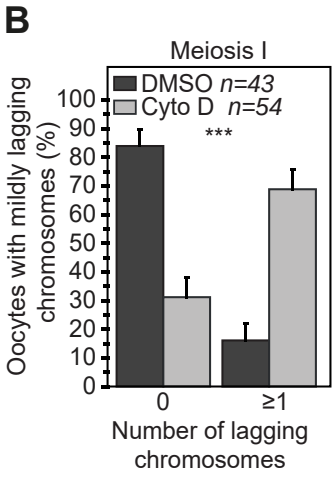
B
Meiosis I
DMSO n=43
Cyto D n=54
***
Oocytes with mildly lagging chromosomes (%)
0
≥1
Number of lagging chromosomes

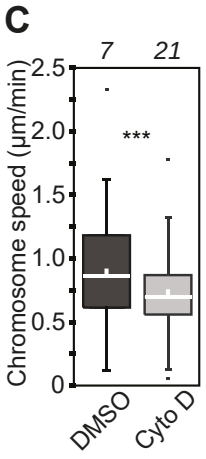
C
7
21
***
Chromosome speed (µm/min)
DMSO
Cyto D

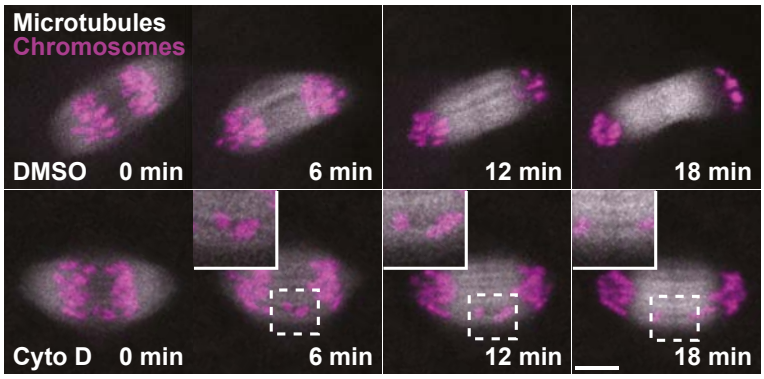
D
Microtubules
Chromosomes
DMSO
Cyto D
0 min
6 min
12 min
18 min

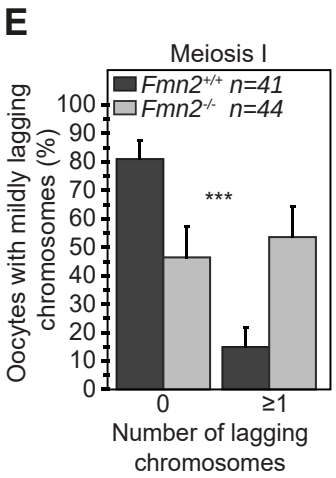
E
Meiosis I
Fmn2+/+ n=41
Fmn2-/- n=44
***
Oocytes with mildly lagging chromosomes (%)
0
≥1
Number of lagging chromosomes

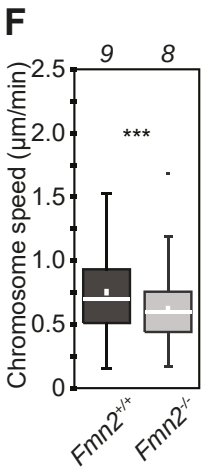
F
9
8
***
Chromosome speed (µm/min)
Fmn2+/+
Fmn2-/-

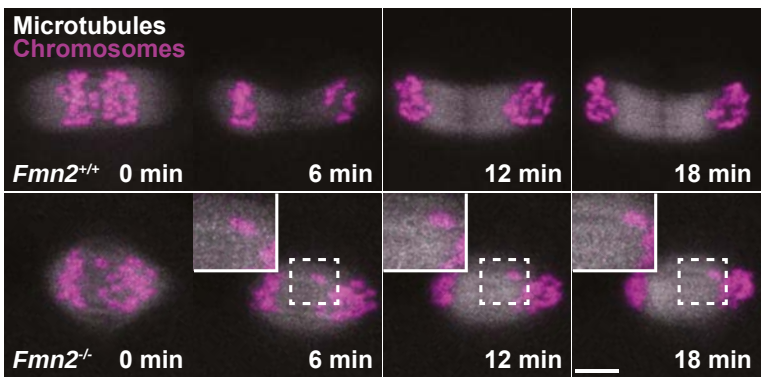
G
Microtubules
Chromosomes
Fmn2+/+
Fmn2-/-
0 min
6 min
12 min
18 min

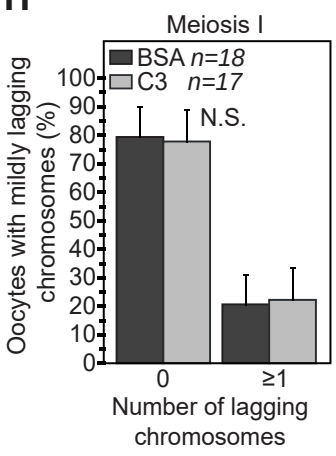
H
Meiosis I
BSA n=18
C3 n=17
N.S.
Oocytes with mildly lagging chromosomes (%)
0
≥1
Number of lagging chromosomes

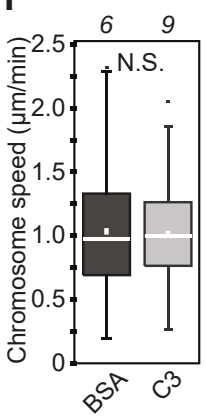
I
6
9
N.S.
Chromosome speed (µm/min)
BSA
C3

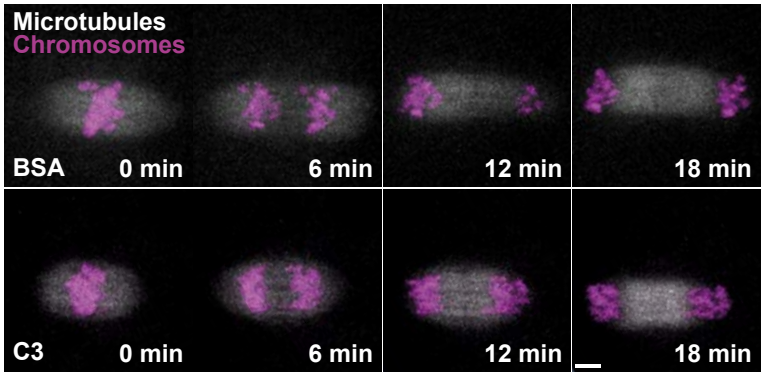
J
Microtubules
Chromosomes
BSA
C3
0 min
6 min
12 min
18 min

Fig. 3

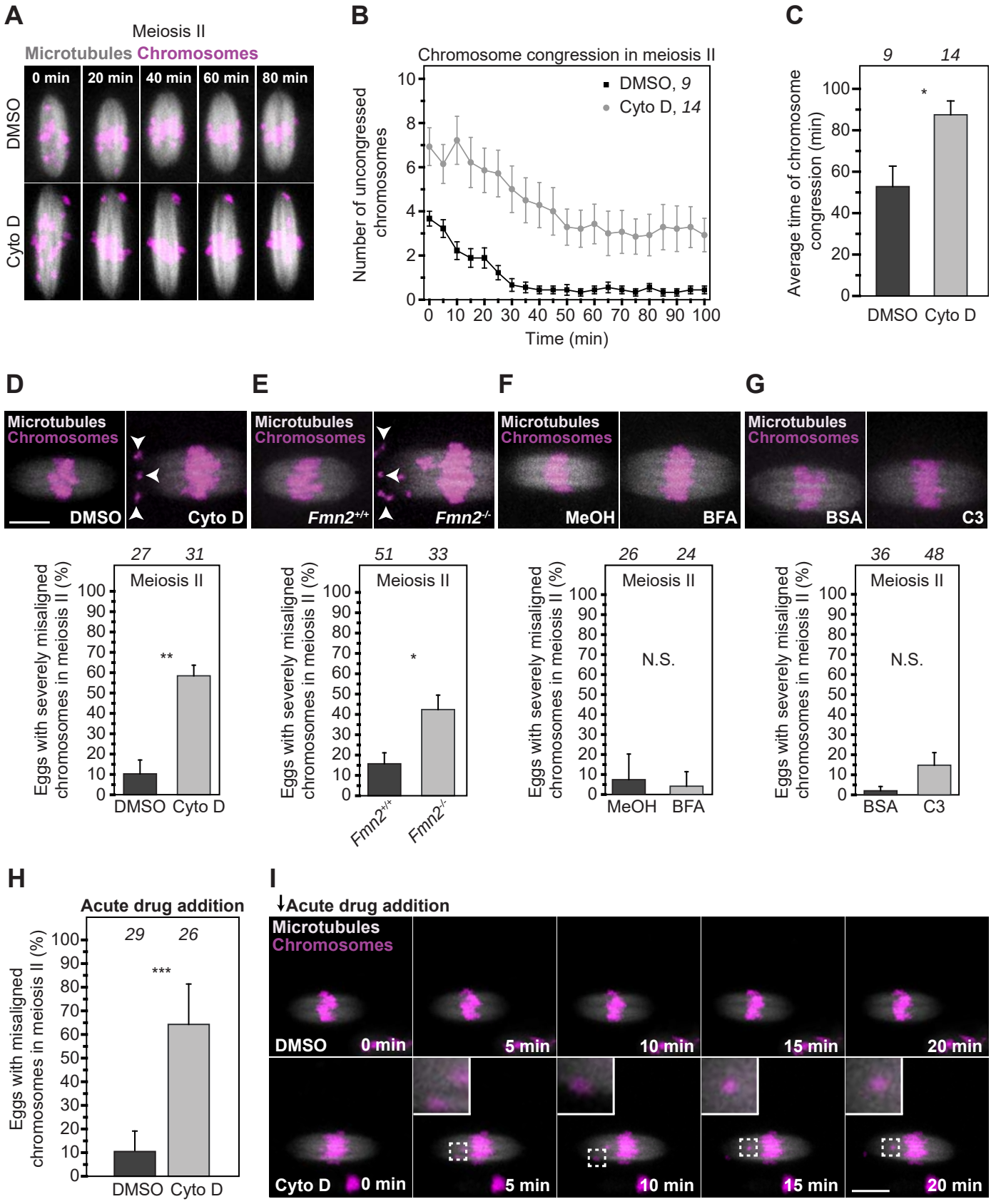
A
Meiosis II
Microtubules Chromosomes
0 min
20 min
40 min
60 min
80 min
DMSO
Cyto D
B
Chromosome congression in meiosis II
DMSO, 9
Cyto D, 14
Number of uncongressed chromosomes
Time (min)
C
9
14
Average time of chromosome congression (min)
DMSO
Cyto D
D
Microtubules
Chromosomes
DMSO
Cyto D
E
Fmn2+/+
Fmn2-/-
F
MeOH
BFA
G
BSA
C3
Eggs with severely misaligned chromosomes in meiosis II (%)
Meiosis II
27
31
51
33
26
24
36
48
N.S.
H
Acute drug addition
29
26
Eggs with misaligned chromosomes in meiosis II (%)
I
Acute drug addition
0 min
5 min
10 min
15 min
20 min

Fig. 4

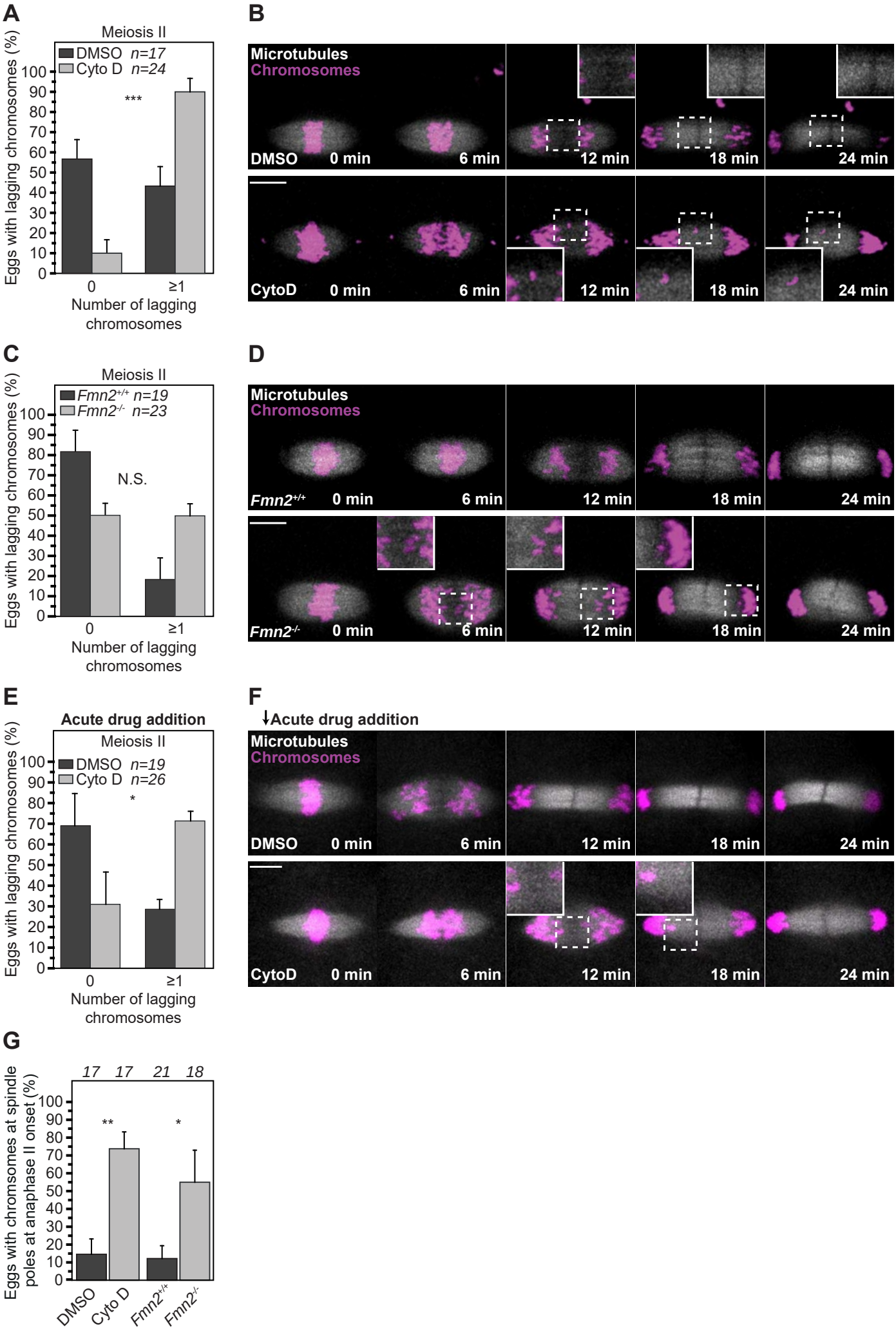
A
Meiosis II
DMSO n=17
Cyto D n=24
***
Eggs with lagging chromosomes (%)
Number of lagging chromosomes
B
Microtubules
Chromosomes
DMSO
CytoD
0 min
6 min
12 min
18 min
24 min
C
Meiosis II
Fmn2+/+ n=19
Fmn2-/- n=23
N.S.
D
Fmn2+/+
Fmn2-/-
E
Acute drug addition
Meiosis II
DMSO n=19
Cyto D n=26
*
F
Acute drug addition
G
17 17 21 18
**
*
Eggs with chromsomes at spindle poles at anaphase II onset (%)
DMSO
Cyto D
Fmn2+/+
Fmn2-/-

Fig. 5

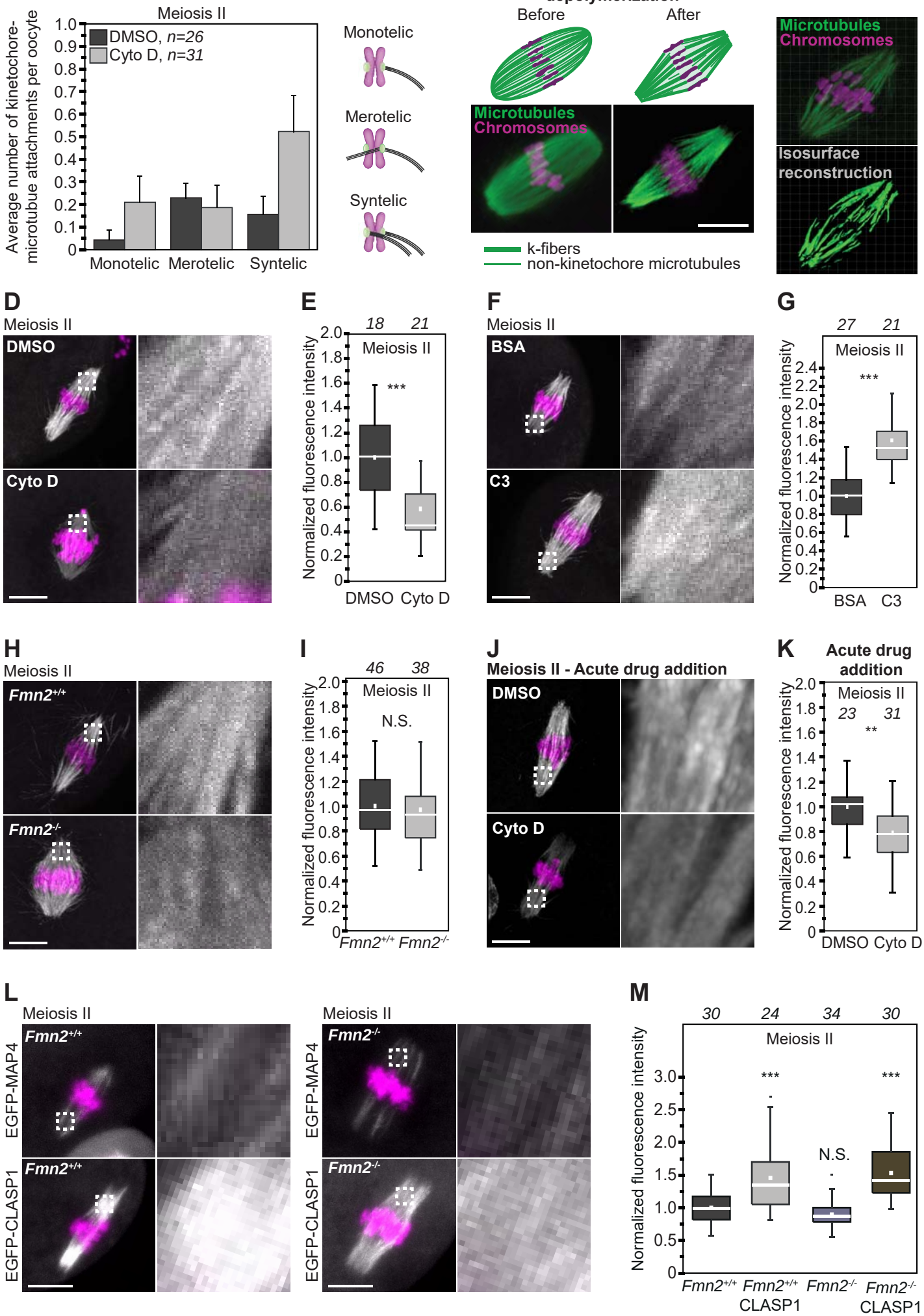
A
Meiosis II
DMSO, n=26
Cyto D, n=31
Average number of kinetochore-microtubue attachments per oocyte
Monotelic
Merotelic
Syntelic
B
Cold-mediated microtubule depolymerization
Before
After
Microtubules
Chromosomes
k-fibers
non-kinetochore microtubules
C
Microtubules
Chromosomes
Isosurface reconstruction
D
Meiosis II
DMSO
Cyto D
E
18
21
Meiosis II
***
Normalized fluorescence intensity
DMSO
Cyto D
F
Meiosis II
BSA
C3
G
27
21
Meiosis II
***
Normalized fluorescence intensity
BSA
C3
H
Meiosis II
Fmn2+/+
Fmn2-/-
I
46
38
Meiosis II
N.S.
Normalized fluorescence intensity
Fmn2+/+
Fmn2-/-
J
Meiosis II - Acute drug addition
DMSO
Cyto D
K
Acute drug addition
Meiosis II
23
31
**
Normalized fluorescence intensity
DMSO
Cyto D
L
Meiosis II
Fmn2+/+
Fmn2-/-
EGFP-MAP4
EGFP-CLASP1
M
30
24
34
30
Meiosis II
***
N.S.
***
Normalized fluorescence intensity
Fmn2+/+
Fmn2+/+
Fmn2-/-
Fmn2-/-
CLASP1
CLASP1

Fig. 6

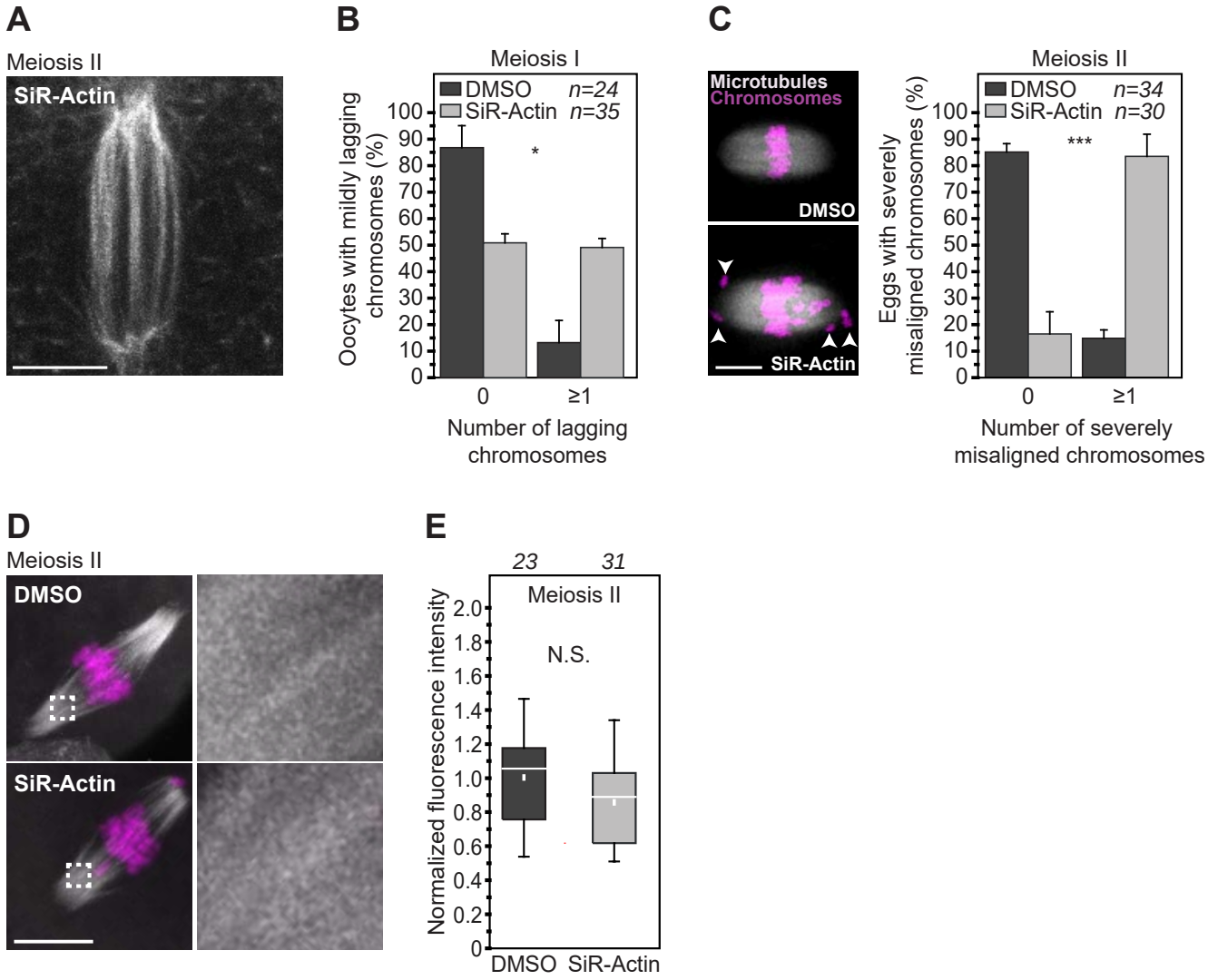
A
Meiosis II
SiR-Actin
B
Meiosis I
DMSO n=24
SiR-Actin n=35
Oocytes with mildly lagging chromosomes (%)
*
0
≥1
Number of lagging chromosomes
C
Microtubules
Chromosomes
DMSO
SiR-Actin
Meiosis II
DMSO n=34
SiR-Actin n=30
Eggs with severely misaligned chromosomes (%)
***
0
≥1
Number of severely misaligned chromosomes
D
Meiosis II
DMSO
SiR-Actin
E
23
31
Meiosis II
N.S.
Normalized fluorescence intensity
DMSO
SiR-Actin

Fig. 7

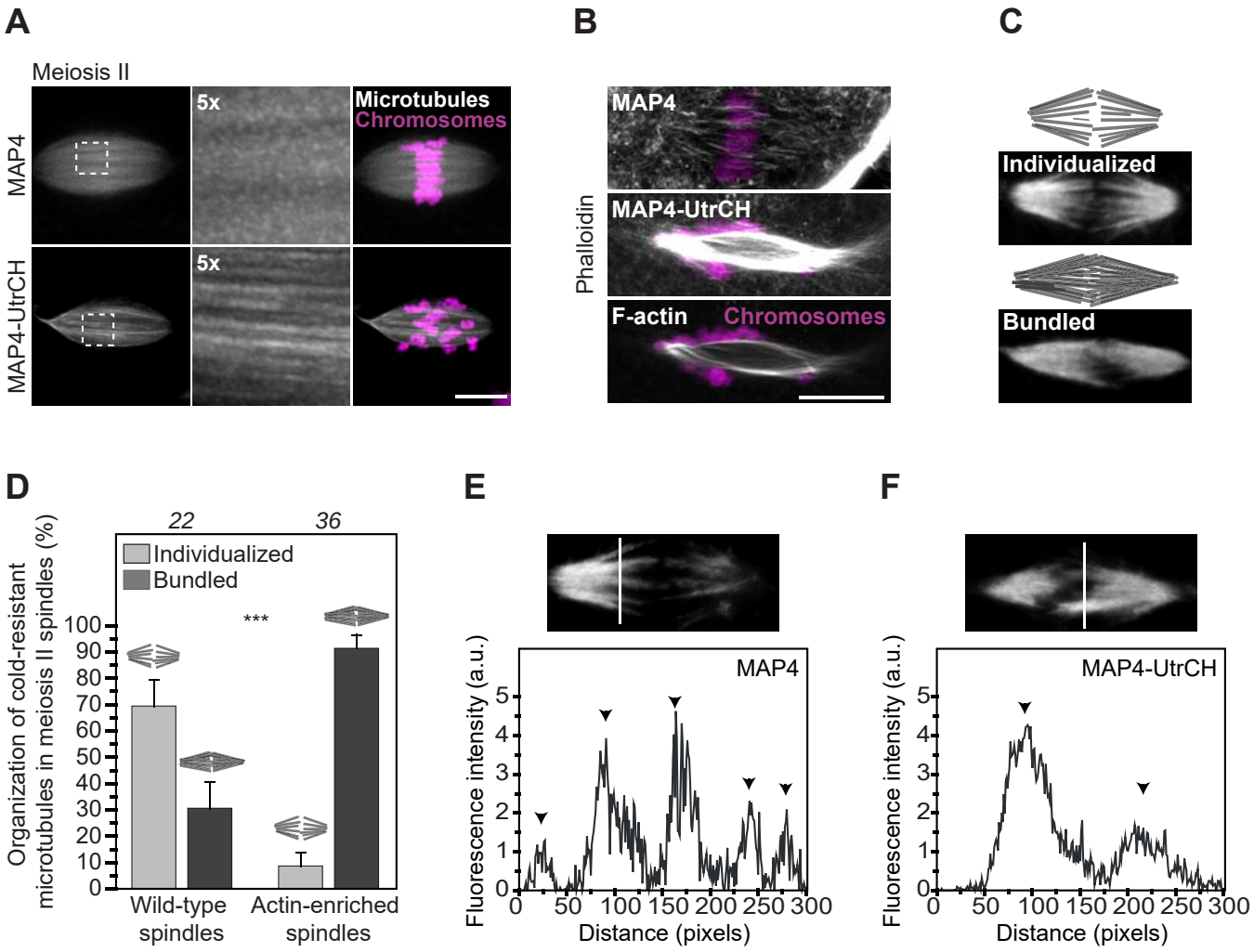
A
Meiosis II
MAP4
MAP4-UtrCH
5x
5x
Microtubules
Chromosomes
B
Phalloidin
MAP4
MAP4-UtrCH
F-actin
Chromosomes
C
Individualized
Bundled
D
22
36
Individualized
Bundled
***
Organization of cold-resistant microtubules in meiosis II spindles (%)
Wild-type spindles
Actin-enriched spindles
E
MAP4
Fluorescence intensity (a.u.)
Distance (pixels)
F
MAP4-UtrCH
Fluorescence intensity (a.u.)
Distance (pixels)

Fig. 8

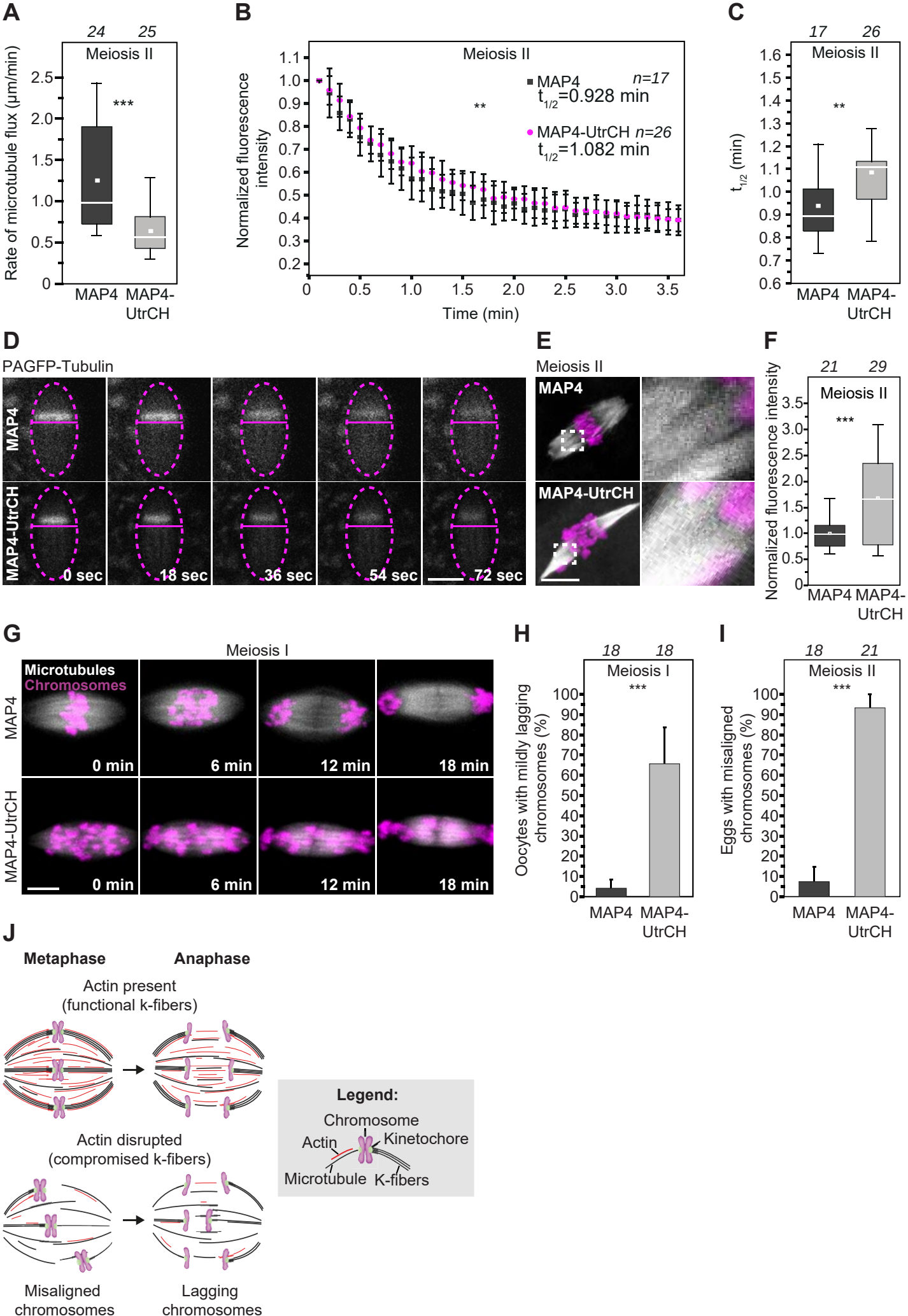
A
24
25
Meiosis II
Rate of microtubule flux (µm/min)
***
MAP4
MAP4-UtrCH
B
Meiosis II
Normalized fluorescence intensity
**
MAP4 n=17
t1/2=0.928 min
MAP4-UtrCH n=26
t1/2=1.082 min
Time (min)
C
17
26
Meiosis II
t1/2 (min)
**
MAP4
MAP4-UtrCH
D
PAGFP-Tubulin
MAP4
MAP4-UtrCH
0 sec
18 sec
36 sec
54 sec
72 sec
E
Meiosis II
MAP4
MAP4-UtrCH
F
21
29
Meiosis II
Normalized fluorescence intensity
***
MAP4
MAP4-UtrCH
G
Meiosis I
Microtubules
Chromosomes
MAP4
MAP4-UtrCH
0 min
6 min
12 min
18 min
H
18
18
Meiosis I
Oocytes with mildly lagging chromosomes (%)
***
MAP4
MAP4-UtrCH
I
18
21
Meiosis II
Eggs with misaligned chromosomes (%)
***
MAP4
MAP4-UtrCH
J
Metaphase
Anaphase
Actin present
(functional k-fibers)
Actin disrupted
(compromised k-fibers)
Misaligned chromosomes
Lagging chromosomes
Legend:
Chromosome
Actin
Kinetochore
Microtubule
K-fibers

Fig S1

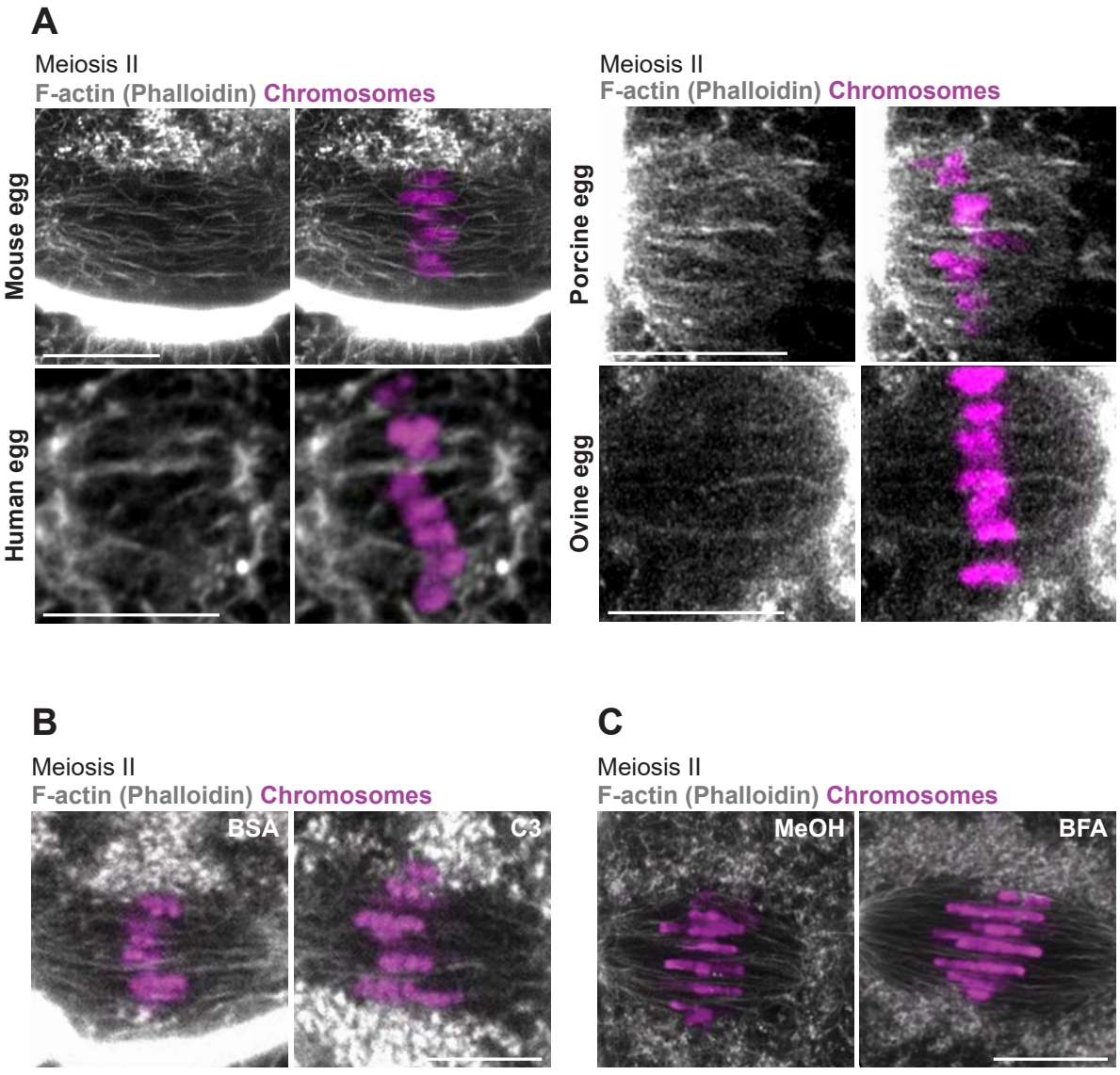
A
Meiosis II
F-actin (Phalloidin) Chromosomes
Mouse egg
Human egg
Meiosis II
F-actin (Phalloidin) Chromosomes
Porcine egg
Ovine egg
B
Meiosis II
F-actin (Phalloidin) Chromosomes
BSA
C3
C
Meiosis II
F-actin (Phalloidin) Chromosomes
MeOH
BFA

Fig S2

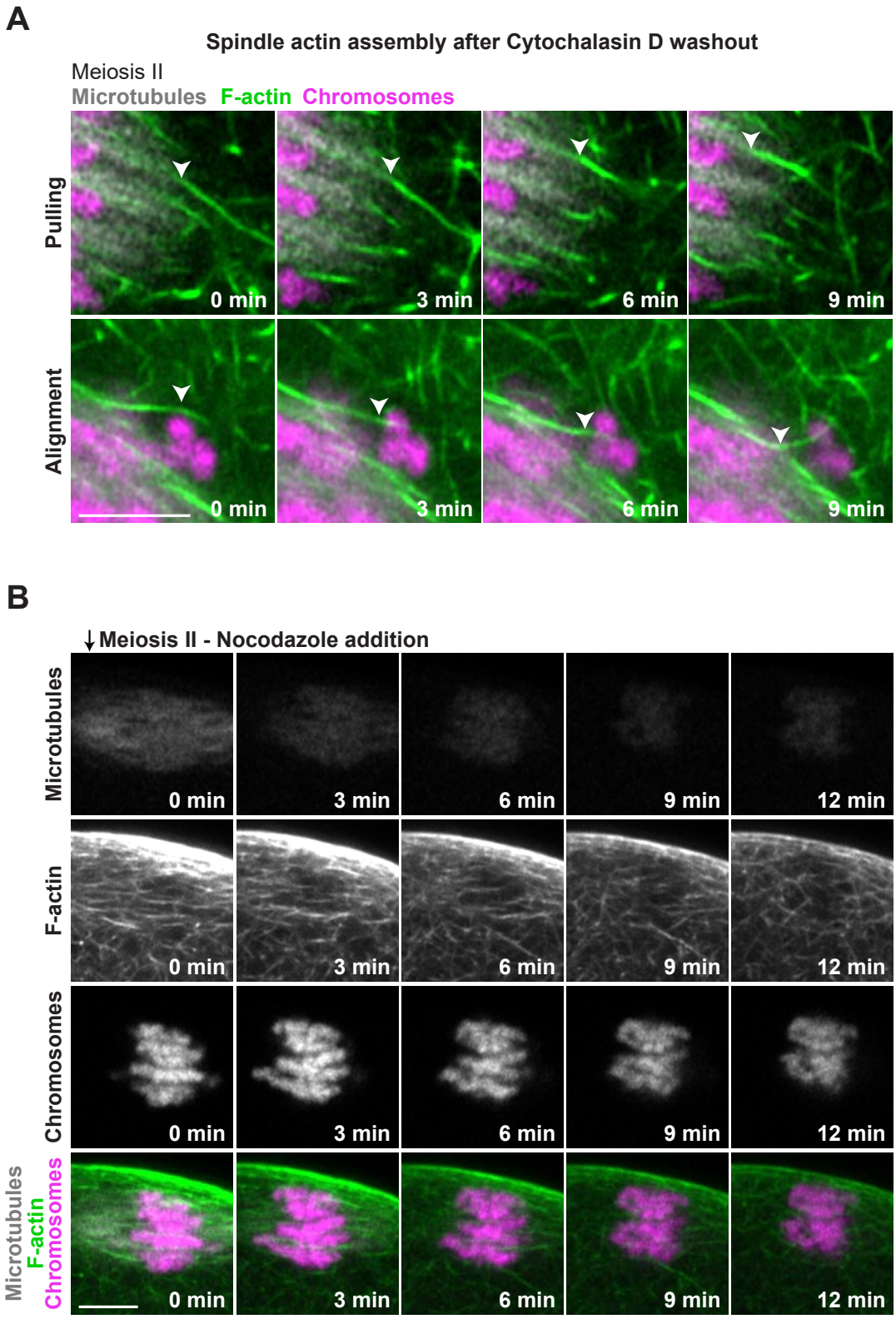
A
Spindle actin assembly after Cytochalasin D washout
Meiosis II
Microtubules F-actin Chromosomes
Pulling
Alignment
0 min
3 min
6 min
9 min
B
Meiosis II - Nocodazole addition
Microtubules
F-actin
Chromosomes
Microtubules
F-actin
Chromosomes
0 min
3 min
6 min
9 min
12 min

Fig S3

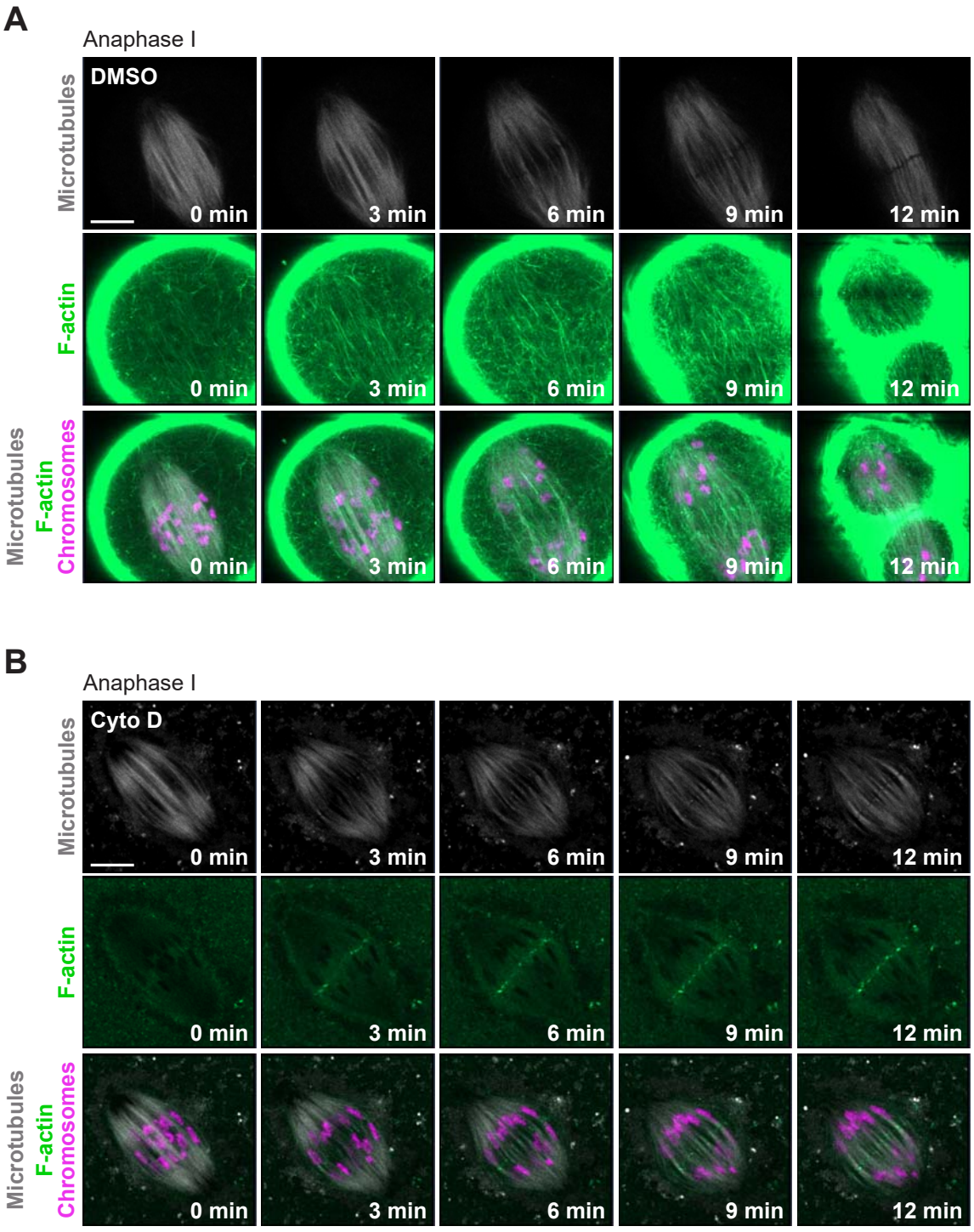
A
Anaphase I
DMSO
Microtubules
F-actin
Microtubules
F-actin
Chromosomes
0 min
3 min
6 min
9 min
12 min
B
Anaphase I
Cyto D
Microtubules
F-actin
Microtubules
F-actin
Chromosomes
0 min
3 min
6 min
9 min
12 min

Fig S4

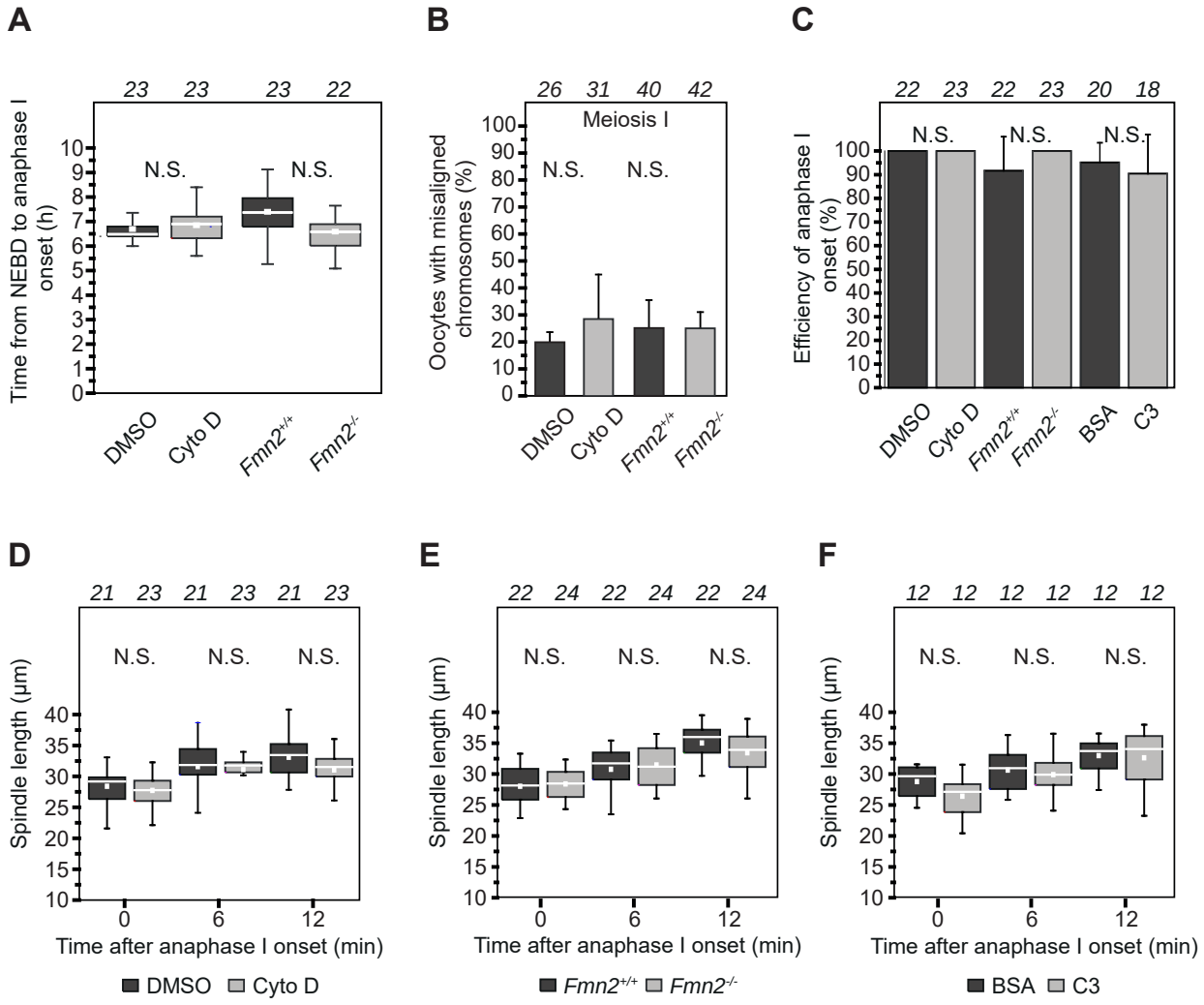
A
B
C
D
E
F
Time from NEBD to anaphase I onset (h)
Oocytes with misaligned chromosomes (%)
Meiosis I
Efficiency of anaphase I onset (%)
N.S.
DMSO
Cyto D
Fmn2+/+
Fmn2-/-
BSA
C3
Spindle length (µm)
Time after anaphase I onset (min)

Fig S5

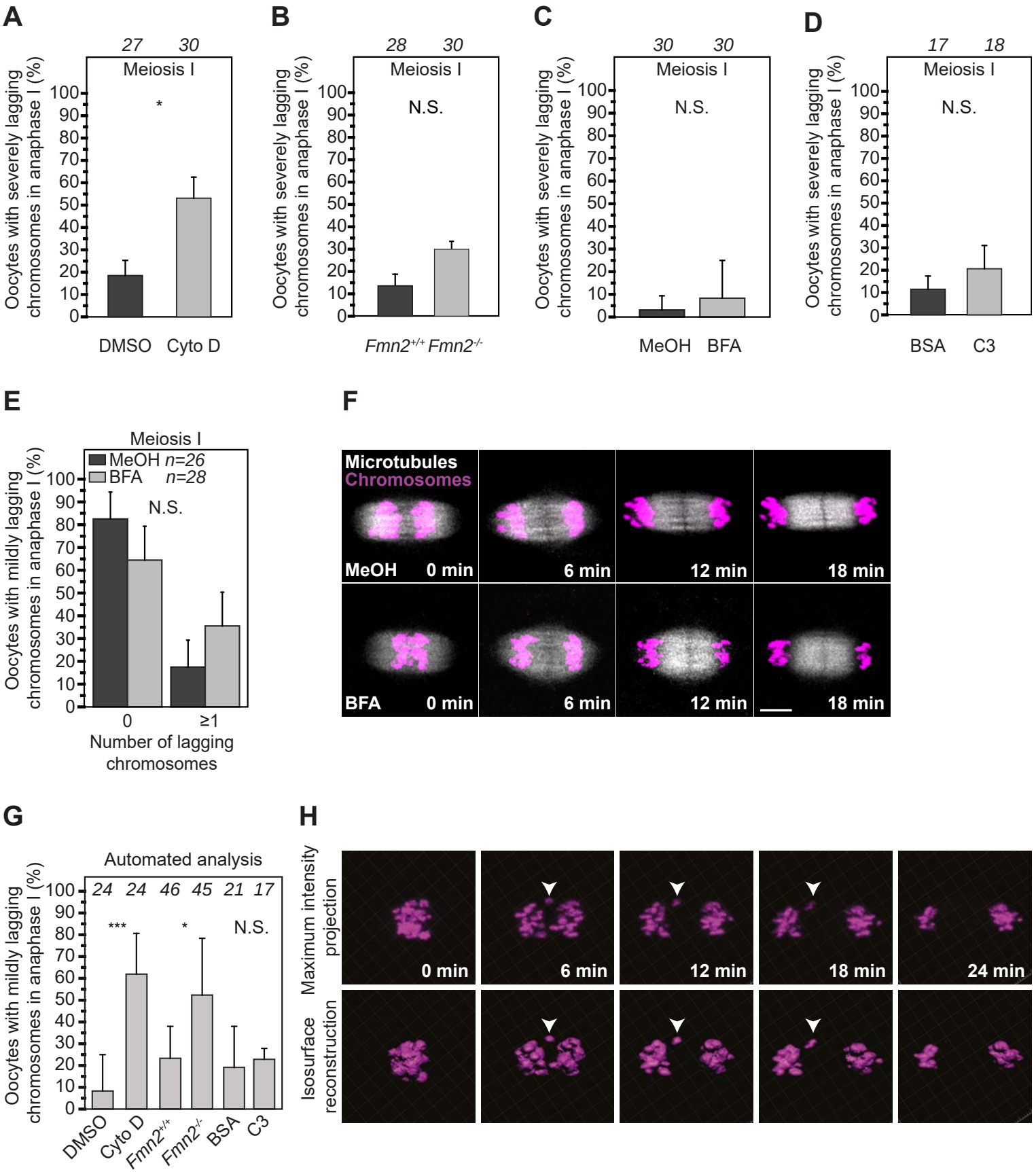
A
27 30
Meiosis I
*
Oocytes with severely lagging chromosomes in anaphase I (%)
DMSO Cyto D
B
28 30
Meiosis I
N.S.
Fmn2+/+ Fmn2-/-
C
30 30
Meiosis I
N.S.
MeOH BFA
D
17 18
Meiosis I
N.S.
BSA C3
E
Meiosis I
MeOH n=26
BFA n=28
N.S.
Oocytes with mildly lagging chromosomes in anaphase I (%)
0 ≥1
Number of lagging chromosomes
F
Microtubules
Chromosomes
MeOH 0 min 6 min 12 min 18 min
BFA 0 min 6 min 12 min 18 min
G
Automated analysis
24 24 46 45 21 17
*** * N.S.
Oocytes with mildly lagging chromosomes in anaphase I (%)
DMSO Cyto D Fmn2+/+ Fmn2-/- BSA C3
H
Maximum intensity projection
Isosurface reconstruction
0 min 6 min 12 min 18 min 24 min

Fig S6

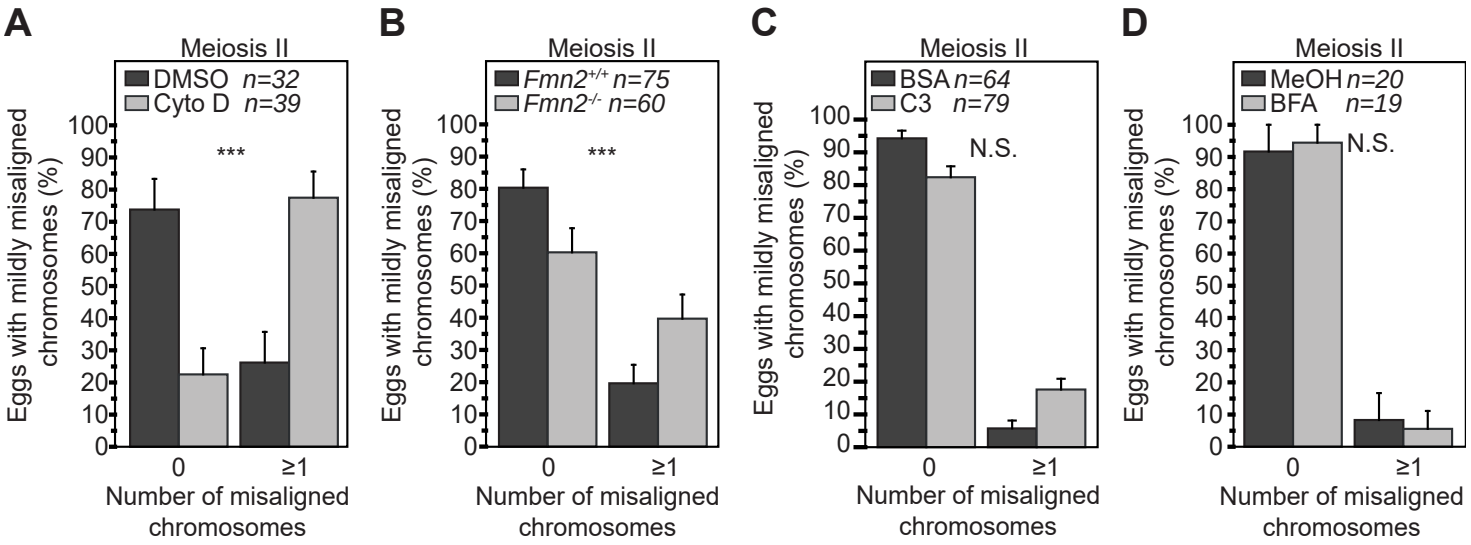
A
Meiosis II
DMSO n=32
Cyto D n=39
***
Eggs with mildly misaligned chromosomes (%)
Number of misaligned chromosomes
B
Meiosis II
Fmn2+/+ n=75
Fmn2-/- n=60
***
C
Meiosis II
BSA n=64
C3 n=79
N.S.
D
Meiosis II
MeOH n=20
BFA n=19
N.S.

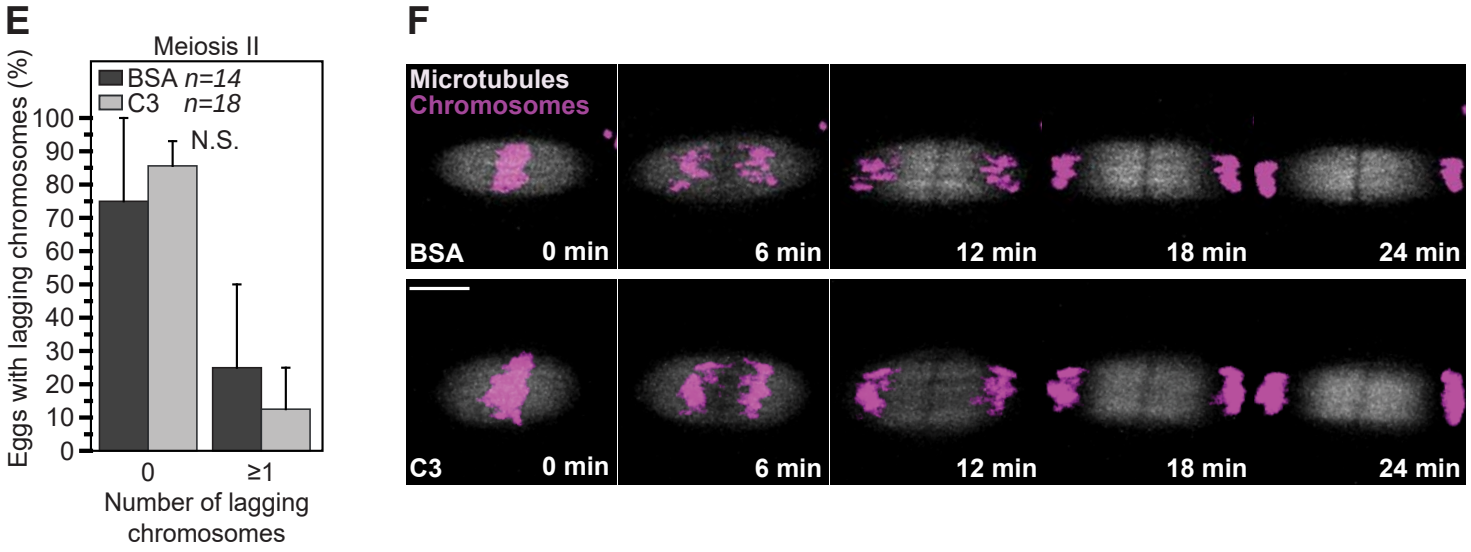
E
Meiosis II
BSA n=14
C3 n=18
N.S.
Eggs with lagging chromosomes (%)
Number of lagging chromosomes
F
Microtubules
Chromosomes
BSA
C3
0 min
6 min
12 min
18 min
24 min

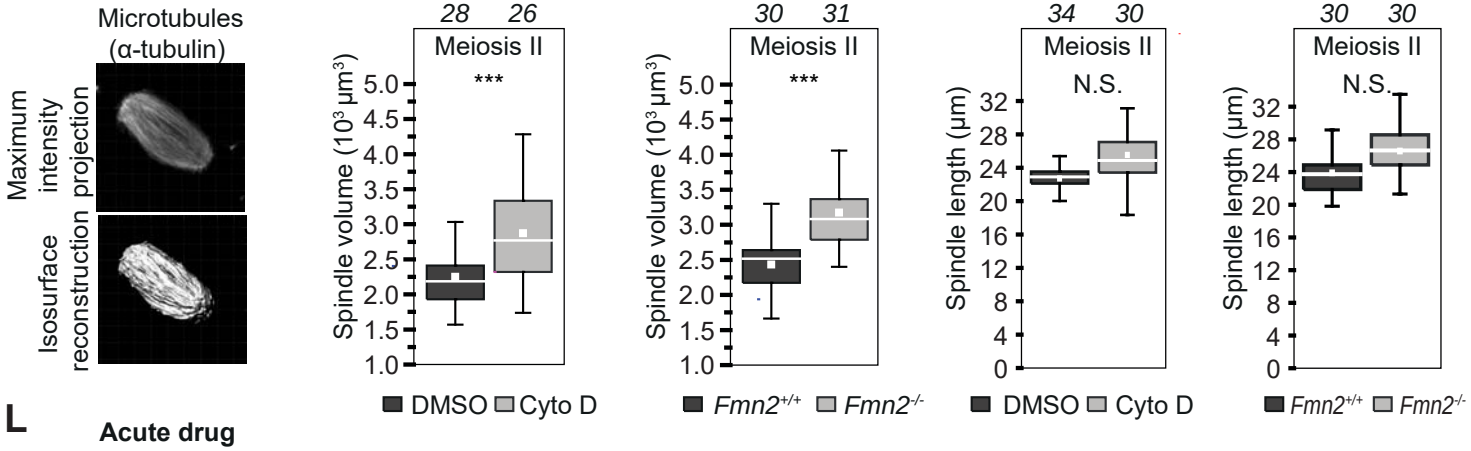
G
Microtubules (α-tubulin)
Maximum intensity projection
Isosurface reconstruction
H
28 26
Meiosis II
***
Spindle volume (10³ µm³)
DMSO Cyto D
I
30 31
Meiosis II
***
Fmn2+/+ Fmn2-/-
J
34 30
Meiosis II
N.S.
Spindle length (µm)
DMSO Cyto D
K
30 30
Meiosis II
N.S.
Fmn2+/+ Fmn2-/-

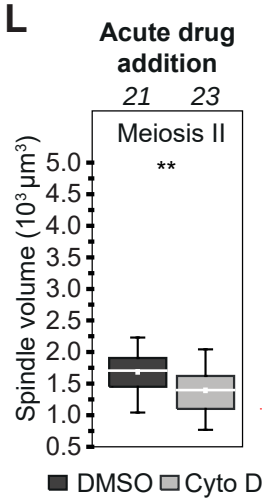
L
Acute drug addition
21 23
Meiosis II
**
Spindle volume (10³ µm³)
DMSO Cyto D

Fig S7

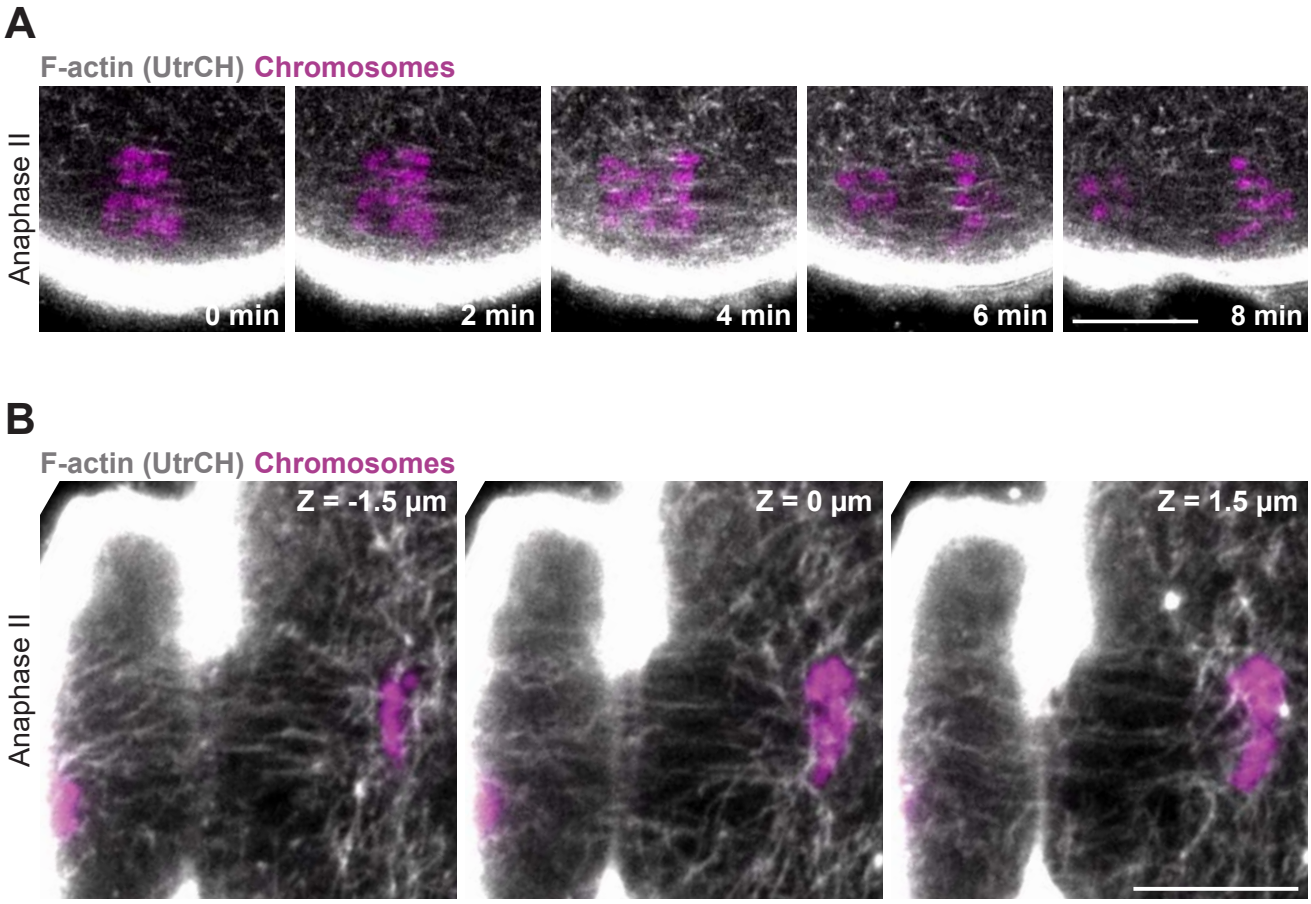
A
F-actin (UtrCH) Chromosomes
Anaphase II
0 min
2 min
4 min
6 min
8 min
B
F-actin (UtrCH) Chromosomes
Anaphase II
Z = -1.5 µm
Z = 0 µm
Z = 1.5 µm

Fig S8

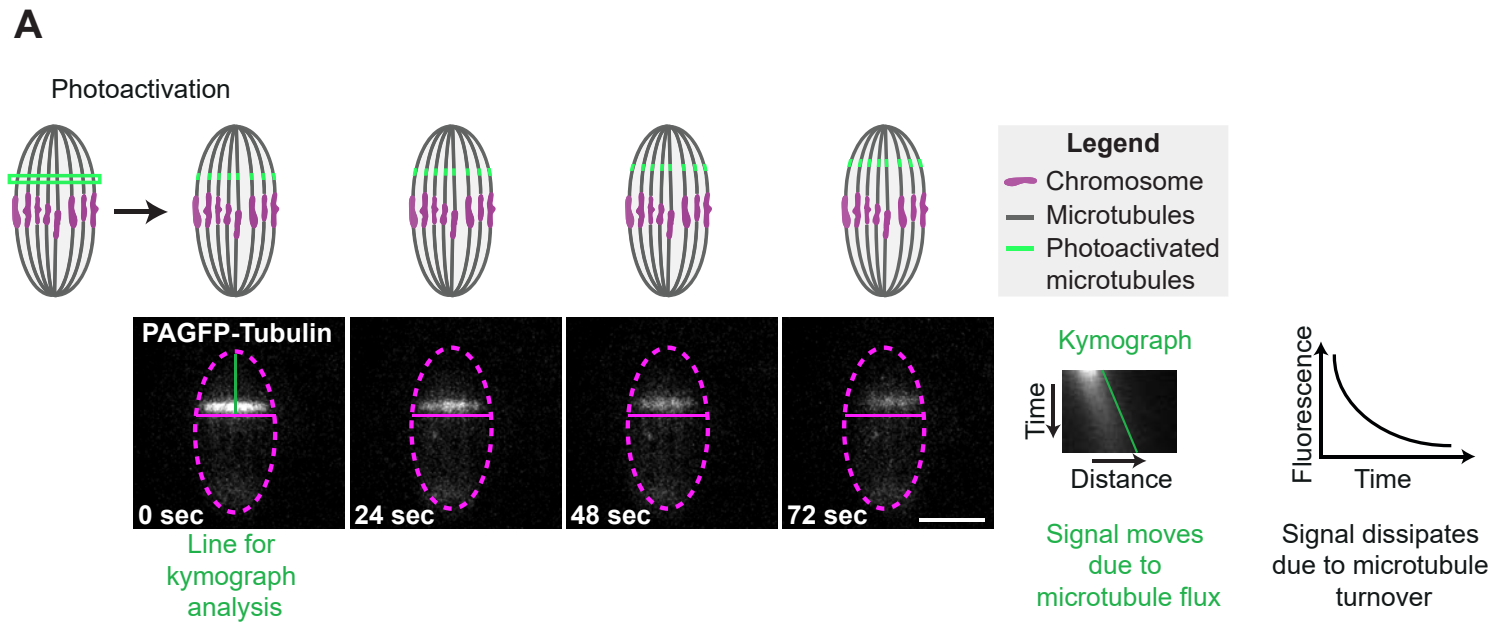
A
Photoactivation
Legend
Chromosome
Microtubules
Photoactivated microtubules
PAGFP-Tubulin
0 sec
24 sec
48 sec
72 sec
Line for kymograph analysis
Kymograph
Time
Distance
Signal moves due to microtubule flux
Fluorescence
Time
Signal dissipates due to microtubule turnover

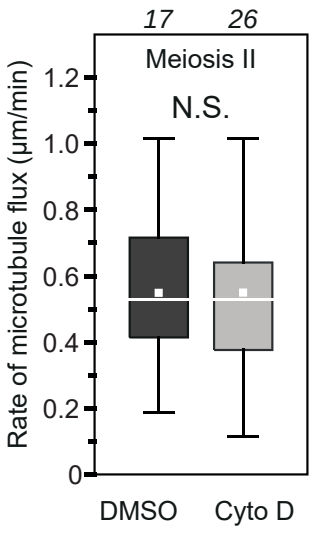
B
17
26
Meiosis II
N.S.
Rate of microtubule flux (µm/min)
1.2
1.0
0.8
0.6
0.4
0.2
0
DMSO
Cyto D

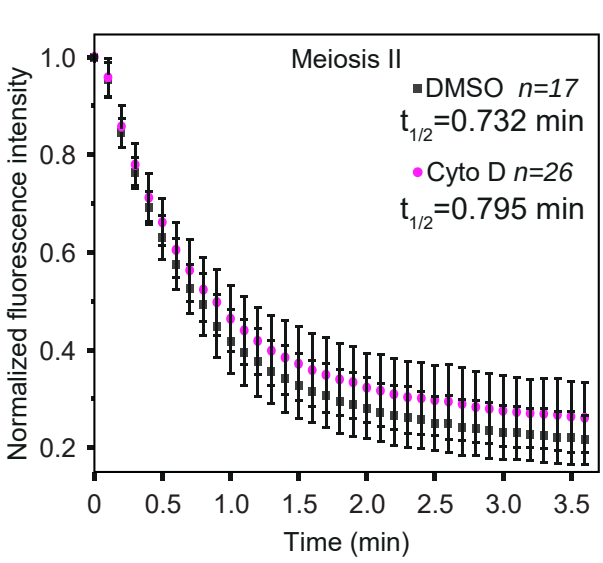
C
Meiosis II
DMSO n=17
t1/2=0.732 min
Cyto D n=26
t1/2=0.795 min
Normalized fluorescence intensity
1.0
0.8
0.6
0.4
0.2
0
0.5
1.0
1.5
2.0
2.5
3.0
3.5
Time (min)

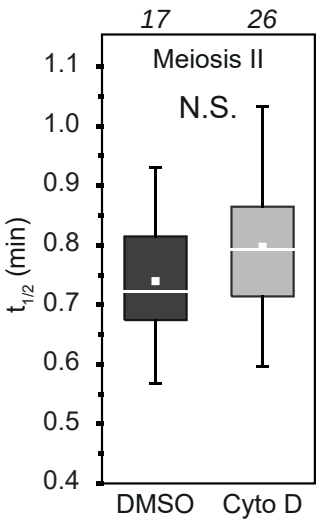
D
17
26
Meiosis II
N.S.
t1/2 (min)
1.1
1.0
0.9
0.8
0.7
0.6
0.5
0.4
DMSO
Cyto D

Fig S9

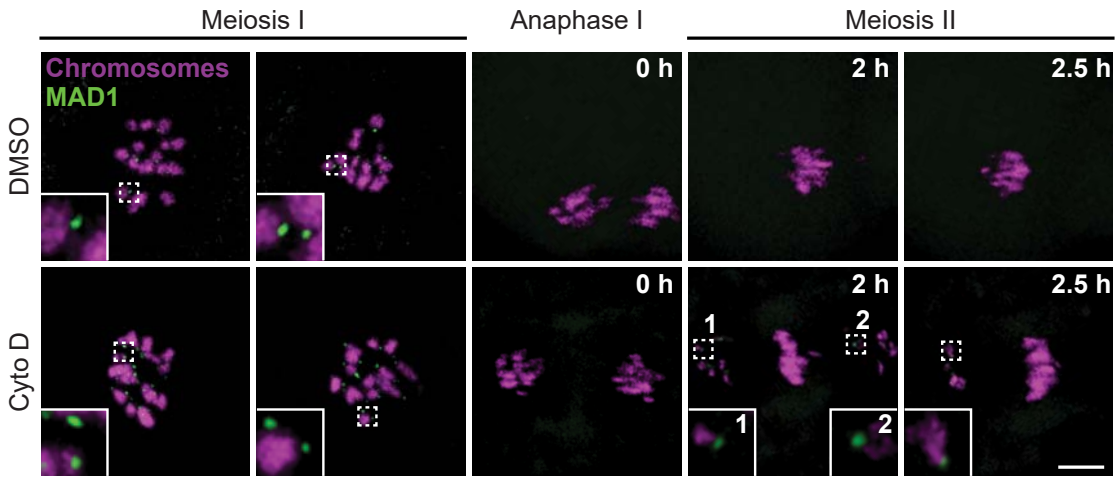
Meiosis I
Anaphase I
Meiosis II
Chromosomes
MAD1
DMSO
Cyto D
0 h
2 h
2.5 h
1
2

Fig S10

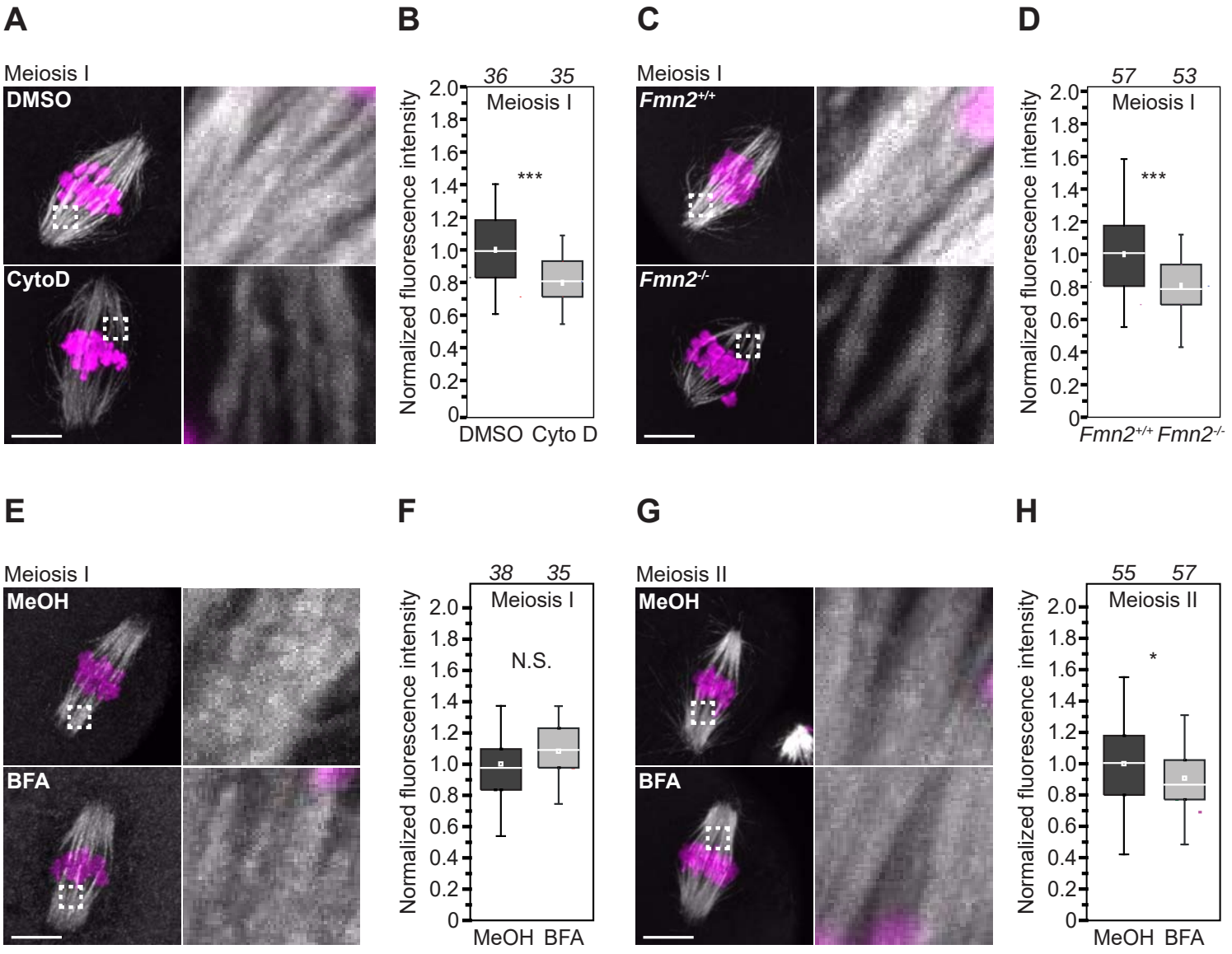
A
Meiosis I
DMSO
CytoD
B
36
35
Meiosis I
***
Normalized fluorescence intensity
2.0
1.8
1.6
1.4
1.2
1.0
0.8
0.6
0.4
0.2
0
DMSO
Cyto D
C
Meiosis I
Fmn2+/+
Fmn2-/-
D
57
53
Meiosis I
***
Normalized fluorescence intensity
Fmn2+/+
Fmn2-/-
E
Meiosis I
MeOH
BFA
F
38
35
Meiosis I
N.S.
Normalized fluorescence intensity
MeOH
BFA
G
Meiosis II
MeOH
BFA
H
55
57
Meiosis II
*
Normalized fluorescence intensity
MeOH
BFA

Fig S11

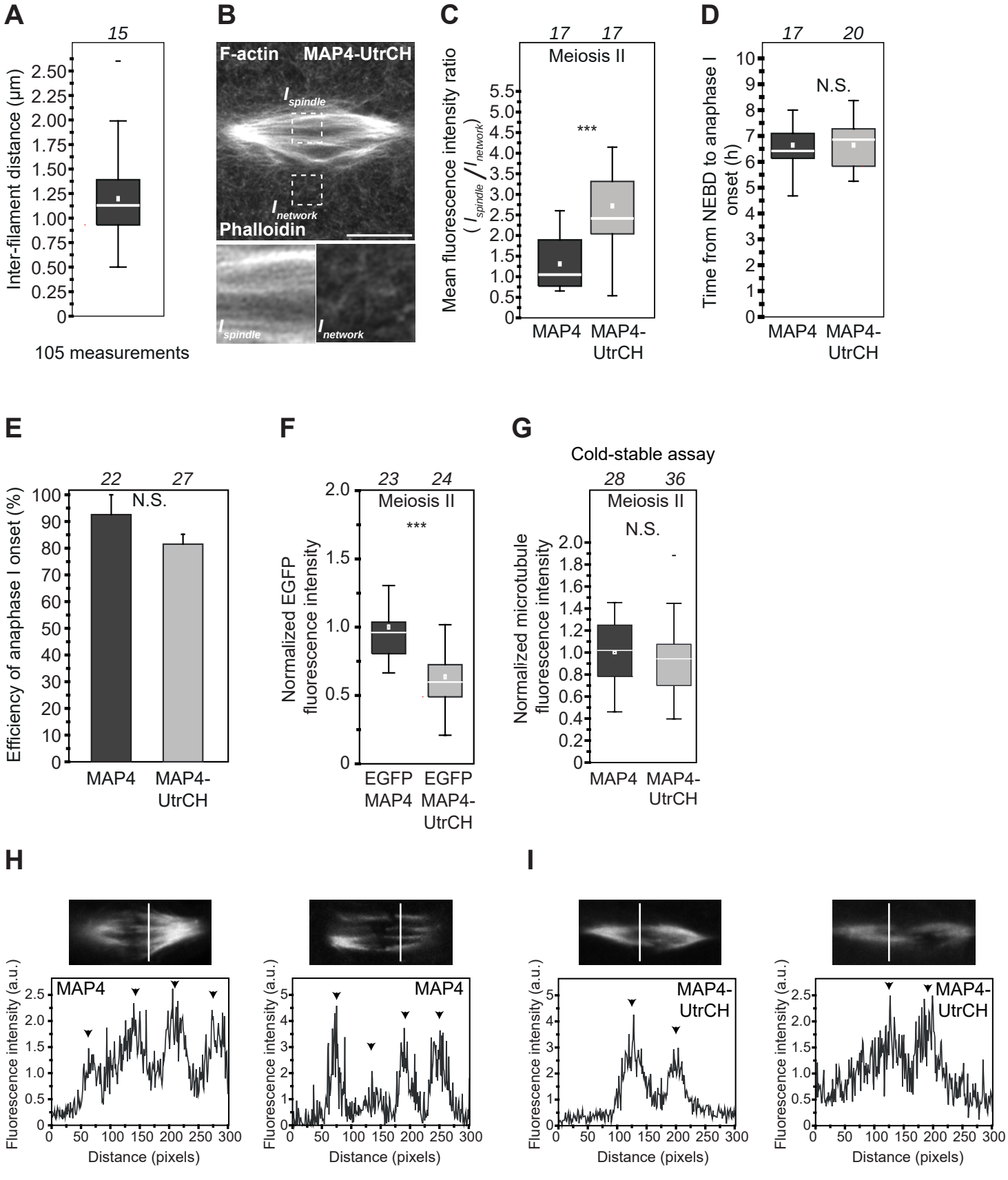
A
15
Inter-filament distance (μm)
105 measurements
B
F-actin
MAP4-UtrCH
I spindle
I network
Phalloidin
C
17 17
Meiosis II
***
Mean fluorescence intensity ratio (I spindle / I network)
MAP4
MAP4-UtrCH
D
17 20
N.S.
Time from NEBD to anaphase I onset (h)
E
22 27
N.S.
Efficiency of anaphase I onset (%)
F
23 24
Meiosis II
***
Normalized EGFP fluorescence intensity
EGFP MAP4
EGFP MAP4-UtrCH
G
Cold-stable assay
28 36
Meiosis II
N.S.
Normalized microtubule fluorescence intensity
H
MAP4
Fluorescence intensity (a.u.)
Distance (pixels)
I
MAP4-UtrCH